NASA/CR-2006-214299
NIA Report No. 2006-02

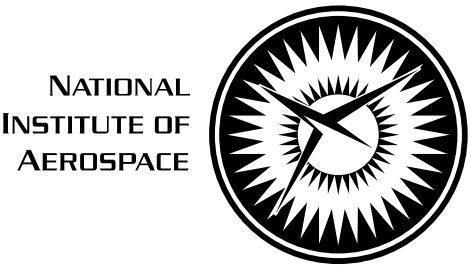

Analysis of Composite Panel-Stiffener Debonding Using a Shell/3D Modeling Technique

Ronald Krueger
National Institute of Aerospace, Hampton, Virginia

Pierre J. Minguet
The Boeing Company, Philadelphia, Pennsylvania

April 2006

The NASA STI Program Office . . . in Profile

Since its founding, NASA has been dedicated to the advancement of aeronautics and space science. The NASA Scientific and Technical Information (STI) Program Office plays a key part in helping NASA maintain this important role.

The NASA STI Program Office is operated by Langley Research Center, the lead center for NASA's scientific and technical information. The NASA STI Program Office provides access to the NASA STI Database, the largest collection of aeronautical and space science STI in the world. The Program Office is also NASA's institutional mechanism for disseminating the results of its research and development activities. These results are published by NASA in the NASA STI Report Series, which includes the following report types:

- TECHNICAL PUBLICATION. Reports of completed research or a major significant phase of research that present the results of NASA programs and include extensive data or theoretical analysis. Includes compilations of significant scientific and technical data and information deemed to be of continuing reference value. NASA counterpart of peer-reviewed formal professional papers, but having less stringent limitations on manuscript length and extent of graphic presentations.

- TECHNICAL MEMORANDUM. Scientific and technical findings that are preliminary or of specialized interest, e.g., quick release reports, working papers, and bibliographies that contain minimal annotation. Does not contain extensive analysis.

- CONTRACTOR REPORT. Scientific and technical findings by NASA-sponsored contractors and grantees.

- CONFERENCE PUBLICATION. Collected papers from scientific and technical conferences, symposia, seminars, or other meetings sponsored or co-sponsored by NASA.

- SPECIAL PUBLICATION. Scientific, technical, or historical information from NASA programs, projects, and missions, often concerned with subjects having substantial public interest.

- TECHNICAL TRANSLATION. English-language translations of foreign scientific and technical material pertinent to NASA's mission.

Specialized services that complement the STI Program Office's diverse offerings include creating custom thesauri, building customized databases, organizing and publishing research results ... even providing videos.

For more information about the NASA STI Program Office, see the following:

- Access the NASA STI Program Home Page at ***http://www.sti.nasa.gov***

- E-mail your question via the Internet to help@sti.nasa.gov

- Fax your question to the NASA STI Help Desk at (301) 621-0134

- Phone the NASA STI Help Desk at (301) 621-0390

- Write to:
  NASA STI Help Desk
  NASA Center for AeroSpace Information
  7121 Standard Drive
  Hanover, MD 21076-1320

NASA/CR-2006-214299
NIA Report No. 2006-02

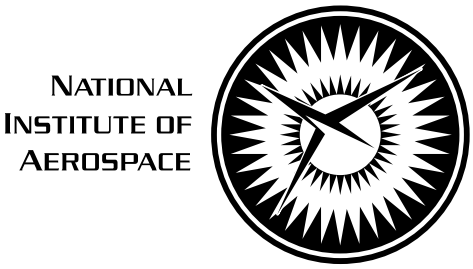

Analysis of Composite Panel-Stiffener Debonding Using a Shell/3D Modeling Technique

Ronald Krueger
National Institute of Aerospace, Hampton, Virginia

Pierre J. Minguet
The Boeing Company, Philadelphia, Pennsylvania

National Aeronautics and
Space Administration

Langley Research Center
Hampton, Virginia 23681-2199

Prepared for Langley Research Center
under Contract NAS1-02117

April 2006

Available from:

NASA Center for AeroSpace Information (CASI)
7121 Standard Drive
Hanover, MD 21076-1320
(301) 621-0390

National Technical Information Service (NTIS)
5285 Port Royal Road
Springfield, VA 22161-2171
(703) 605-6000

ANALYSIS OF COMPOSITE PANEL-STIFFENER DEBONDING USING A SHELL/3D MODELING TECHNIQUE

Ronald Krueger[1] and Pierre J. Minguet[2]

ABSTRACT

Interlaminar fracture mechanics has proven useful for characterizing the onset of delaminations in composites and has been used with limited success primarily to investigate onset in fracture toughness specimens and laboratory size coupon type specimens. Future acceptance of the methodology by industry and certification authorities however, requires the successful demonstration of the methodology on structural level. For this purpose a panel was selected that is reinforced with stringers. Shear loading causes the panel to buckle and the resulting out-of-plane deformations initiate skin/stringer separation at the location of an embedded defect. For finite element analysis, the panel and surrounding load fixture were modeled with shell elements. A small section of the stringer foot and the panel in the vicinity of the embedded defect were modeled with a local 3D solid model. A failure index was calculated by correlating computed mixed-mode strain energy release rates with the mixed-mode failure criterion of the graphite/epoxy material. Computed failure indices were in good agreement with results from models where the entire delaminated section of the stiffener foot had been modeled with solid elements. The shell-to-solid connection influenced the computed failure indices and local refinement of the shell model across the stringer foot and web was required to improve the results. The study confirmed that the section modeled locally did not have to include the entire delaminated section. The use of a smaller local inserts reduced model size without compromising the computed failure indices.

1. BACKGROUND

Many composite components in aerospace structures are made of flat or curved panels with co-cured or adhesively bonded frames and stiffeners. Recent studies focused on the investigation of the debonding mechanism and included testing of composite skin/stiffener panels and failure analysis using shell models [1-4]. Over the last decade a consistent step-wise approach has been developed which uses experiments to detect the failure mechanism, computational stress analysis to determine the location of first matrix cracking and computational fracture mechanics to investigate the potential for delamination growth. Testing of skin gage stiffened panels designed for pressurized aircraft fuselage has shown that bond failure at the tip of the frame flange is an important and very likely failure mode [5]. Comparatively simple specimens consisting of a stringer flange bonded onto a skin have been developed to study skin/stiffener debonding [6-8]. The failure mode that initiates at the tip of the flange in these specimens is nearly identical to the failure mode observed in the full-scale panels and the frame pull-off specimens [7, 9, 10]. A methodology based on fracture mechanics [11] has proven useful for characterizing the onset and growth of delaminations in composites and has been used with limited success to investigate delamination onset and debonding in spimple laboratory coupon type specimens [9, 10]. Future acceptance of a fracture mechanics methodology by

1 National Institute of Aerospace (NIA), 100 Exploration Way, Hampton, VA 23666.

2 The Boeing Company, Philadelphia, Pennsylvania

industry and certification authorities however, requires the successful demonstration of the methodology on structural level.

For the demonstration of a fracture mechanics methodology on structural level, a stringer stiffened panel as shown in Figure 1, had been selected and analyzed in a related study [12]. The square panel is made of IM7/8552 carbon/epoxy tape and reinforced with three stringers made of IM7/8552 carbon/epoxy plain weave fabric. The stiffened panel is bolted to a steel picture frame and subjected to pure in-plane shear loading. A finite element model is shown in Figure 1a. During manufacturing an artificial defect had been placed at the termination of the center stiffener. Sufficient shear loading causes the panel to buckle as shown in Figure 1a. The resulting out-of-plane deformation causes skin/stringer separation at the location of the initial defect as shown in the detail of the deformed mesh in Figure 1b. A total of eight delamination lengths between 81.9 and 355.6 mm were modeled using short and long insert models as shown in Figures 1b and c. The mixed-mode strain energy release rates were calculated using the virtual crack closure technique across the width of the stringer foot. A failure index was calculated by correlating the results with the mixed-mode failure criterion of the graphite/epoxy material [12].

The objective of this research is to establish that the section modeled locally did not have to include the entire delaminated section as shown in Figures 1 b and c. The goal was to use smaller local inserts and thereby reduce model size and CPU time without compromising the computed failure indices. A total of seven delamination lengths between 81.9 and 355.6 mm were modeled and computed failure indices were compared to previous results where the entire delaminated section had been modeled with solid elements [12].

2. METHODOLOGY

2.1. Interlaminar Fracture Mechanics

Interlaminar fracture mechanics has proven useful for characterizing the onset and growth of delaminations [11, 13]. When using fracture mechanics the total strain energy release rate, G_T, the mode I component due to interlaminar tension, G_I, the mode II component due to interlaminar sliding shear, G_{II}, and the mode III component, G_{III}, due to interlaminar scissoring shear, as shown in Figure 2, are calculated along the delamination. The calculated G_I, G_{II}, and G_{III} components are then compared to interlaminar fracture toughness values in order to predict delamination onset or growth. The interlaminar fracture toughness values are determined experimentally over a range of mode mixities from pure mode I loading to pure mode II loading [14-16].

A quasi static mixed-mode fracture criterion is determined by plotting the interlaminar fracture toughness, G_c, versus the mixed-mode ratio, G_{II}/G_T. The fracture toughness data is generated experimentally using pure Mode I (G_{II}/G_T=0) Double Cantilever Beam (DCB), pure Mode II (G_{II}/G_T=1) four point End Notched Flexure (4ENF), and Mixed Mode Bending (MMB) tests of varying ratios as shown in Figure 3 for IM7/8852 carbon epoxy material. A failure criterion was suggested by Benzeggah and Kenane [17] using a simple mathematical relationship between G_c and G_{II}/G_T

$$G_c = G_{Ic} + \left(G_{IIc} - G_{Ic}\right) \cdot \left(\frac{G_{II}}{G_T}\right)^{\eta} . \qquad (1)$$

In this expression G_{Ic} and G_{IIc} are the experimentally-determined fracture toughness data for mode I and II as shown in Figure 3. The factor η was determined by a curve fit using the Levenberg-Marquardt algorithm in KaleidaGraph™. Failure is expected when, for a given mixed mode ratio G_{II}/G_T, the calculated total energy release rate, G_T, exceeds the interlaminar fracture toughness, G_c. Although several specimens have been suggested for the measurement of the mode III interlaminar fracture toughness property [18-20], an interaction criterion incorporating the scissoring shear, however, has not yet been established. The edge-cracked torsion test (ECT) is being considered for standardization [21, 22].

2.2. Analysis Tools

2.2.1 Virtual Crack Closure Technique

A variety of methods are used in the literature to compute the strain energy release rate based on results obtained from finite element analysis. For delaminations in laminated composite materials where the failure criterion is highly dependent on the mixed-mode ratio (as shown in Figure 3) the virtual crack closure technique (VCCT) [23, 24] has been widely used for computing energy release rates. Results based on continuum (2-D) and solid (3-D) finite element analyses provide the mode separation required when using the mixed-mode fracture criterion.

The mode I, and mode II components of the strain energy release rate, G_I, G_{II} are computed as shown in Figure 4 for a 2-D four-noded element as an example of VCCT. The terms X'_i, Z'_i are the forces at the crack tip at nodal point i and u'_ℓ, w'_ℓ (u'_{ℓ^*}, w'_{ℓ^*}) are the displacements at the corresponding nodal points ℓ and ℓ^* behind the crack tip. For geometric nonlinear analysis where large deformations may occur, both forces and displacements obtained in the global coordinate system need to be transformed into a local coordinate system (x', z') which originates at the crack tip as shown in Figure 4. The local crack tip system defines the tangential (x', or mode II) and normal (z', or mode I) coordinate directions at the crack tip in the deformed configuration. The extension to 3-D is straight forward and the total energy release rate G_T is calculated from the individual mode components as $G_T = G_I + G_{II} + G_{III}$, where $G_{III} = 0$ for the two-dimensional case shown in Figure 4.

2.2.2 A Global/Local Shell 3D Modeling Technique

Built-up structures are traditionally modeled and analyzed using plate or shell finite elements as shown in Figure 1a to keep the modeling and computational effort affordable. Computed mixed mode strain energy release rate components, however, depend on many variables such as element order and shear deformation assumptions, kinematic constraints in the neighborhood of the delamination front, and continuity of material properties and section stiffness in the vicinity of the debond when delaminations or debonds are modeled with plate or shell finite elements [25-27]. These problems may be avoided by using three-dimensional models. Since many layers of brick elements through the thickness are often necessary to model the individual plies, however, the size of finite element models required for accurate analyses may become prohibitively large.

For detailed modeling and analysis of the delaminations, the shell/3D modeling technique will reduce the modeling time since existing plate or shell models may be modified to shell/3D models. This is a considerable advantage compared to the creation of an entirely new three-

dimensional finite element model. The technique will also reduce computational time because only a relatively small section of interest needs to modeled with solid elements keeping the number of unknowns small. The technique combines the accuracy of the full three-dimensional solution with the computational efficiency of a plate or shell finite element model and has been demonstrated for various applications such as fracture toughness characterization specimens [28, 29], on coupon level for the skin/stringer separation specimen [30, 31] and recently in a related study for skin/stringer separation [12] as shown in Figure 1.

3. FINITE ELEMENT MODELING

The stringer stiffened panel as shown in Figure 1 is bolted to a steel picture frame and subjected to pure shear loading. For the current study seven delamination lengths (a=81.9 mm, 88.9 mm, 94.9 mm, 101.6 mm, 203.2 mm, 279.4 mm and 355.6 mm) were selected to be reanalyzed with a smaller local 3D insert models to reduce the CPU time. Compared to the local insert models shown in Figure 1, only a small part of the intact and delaminated sections of the stringer were modeled with solid elements.

3.1 Global Shell Model of Stringer Stiffened Panel

The global model representing the steel loadframe, the panel made of graphite/epoxy prepreg tape and the stringers made of graphite/epoxy fabric was created using standard S4 shell elements available in the finite element software ABAQUS®. The outer steel load frame was modeled with beam elements as shown in Figure 5a. The inner steel load frame which overlaps the panel edge was modeled with standard shell S4 elements. Shell elements were also used to model the panel and the stiffener components, such as foot, web and hat. Material data are given in Table 1. Details of the global finite element model are discussed in reference [12].

A detail of the global finite element model in the vicinity of the stringer termination is shown in Figure 5b. In preparation for the global/local modeling approach, shell elements representing the foot of the stiffener and the panel were removed from a small section of the original shell model around the center stringer termination. The shell elements used to model the stiffener web and hat were kept in place. Shell edges (e.g. STRFOOT, STRBOT, PNLEND, PNLLEFT, PNLFRNT) in ABAQUS® were defined as shown, which were used to connect the shell model with the local 3D insert model. The connection was accomplished using the shell to solid coupling option in ABAQUS®, which allows the connection between non-conforming shell and solid models. In the detail it is also clearly visible that the panel skin and the stiffener foot are modeled as separate offset entities. The S4 shell elements are located at the panel skin and stiffener foot respective mid-planes. The shell elements are connected by beam elements designed to enforce plate theory constraints [12]. In the sections containing the artificial defects the beam elements were replaced by gap elements. The gap elements allow the modeling of the skin/stringer separation but also prevent element interpenetration in case the surfaces get into contact during the analysis.

3.2 Local 3D Insert Model for Solid Modeling of the Stringer Foot and Panel Skin

The local 3D insert model was generated using C3D8I solid brick elements and consisted of an intact section and a delaminated section with a fine mesh around the delamination front as

shown in Figure 6a. Surfaces were defined in ABAQUS on the outer faces of the insert model to provide a connection with the global shell model using the shell to solid coupling option in ABAQUS®. The initial defect is located at the bondline between stringer foot and the panel. This defect was treated as a delamination and modeled as a discrete discontinuity using two unconnected nodes with identical coordinates one on each side of the delamination. A refined mesh was used along the stringer boundary in order to capture edge effects as shown in Figure 6b. Using the finite sliding option available in ABAQUS® contact was modeled between the delaminated surfaces to avoid interpenetration during analysis. Four elements over the thickness were used to model the foot of the stiffener made of carbon/epoxy fabric as shown in Figure 6b. The -45° skin ply made carbon/epoxy tape which is adjacent to the plane of delamination was modeled with one element. The remaining 10 plies of carbon/epoxy tape were modeled with three elements over the thickness a shown in Figure 6b.

3.3 Combined Global/Local Shell/3D Model of Stringer Stiffned Panel

For modeling the experiment, which was performed under constant displacement control, uniform displacements *u,v* were applied at one corner node to introduce shear as shown in Figure 7a. The in-plane displacements *u,v* were suppressed at the diagonally opposite corner and the out of plane displacements *w* were suppressed along all four edges across the entire width of the inner and outer steel load frame. The local 3D insert model containing a straight delamination front was inserted into the global shell model as shown in the detail of Figure 7b. The local 3D insert model consisted of an intact section and a delaminated section of length *a* with a fine mesh around the delamination front as discussed above. The global shell model was connected to the local 3D insert model using the shell-to-solid coupling option in ABAQUS® which allows the connection between non-conforming shell and solid models. For the entire analyses the non-linear solution option was used in ABAQUS®.

A total of seven delamination lengths were modeled (*a*=81.9 mm, 88.9 mm, 94.9 mm, 101.6 mm, 203.2 mm, 279.4 mm and 355.6 mm). The initial length corresponds to the length of insert used to create an initial defect at the termination of the center stringer. Additional lengths were chosen to study the change in failure index distribution across the width (*b*) of the stringer with increasing delamination length (*a*). The lengths modeled correspond to the lengths investigated in a related study which was used for comparison [12]. A local 3D insert with a fine mesh near the free edges of the stringer foot is shown in Figures 8a. In the local model only 38.1 mm of the stringer foot and panel skin were modeled with CD8I solid brick elements compared to 116.7 mm in the related study as shown in Figure 1b. The number of element were reduced by 40% as listed in Table 2. Additionally a local 3D insert of the same length but with a uniform mesh across the entire width of the stringer foot was generated. The mesh was used for comparison and is shown in Figure 8b. The delaminated section of the stringer modeled with shell elements and the local 3D insert model used to analyze a delamination length *a*=355.6 mm is shown in Figure 8c. In the local model only 55.6 mm of the stringer foot and panel skin were modeled with CD8I solid brick elements compared to 431.2 mm in the related study [12] as shown in Figure 1c. The number of elements in the local insert could be reduced by nearly 60%. The size of the different solid insert models used is listed in Table 2 for comparison.

4. ANALYSIS RESULTS

4.1 Deformed Finite Element Model for Solid Modeling of the Stringer Foot and Panel Skin

The detail of the deformed local models are shown in Figures 9 and 10 for the last analysis increment after the entire external displacement u=v=6.35 mm had been applied. The detail of the deformed local models for a delamination length a=81.9mm are shown in Figure 9. In Figure 9a the opening gap elements are clearly visible. The gap elements were used to prevent contact in the delaminated section modeled with shell elements. For clarity the gap elements are not displayed for the remainder of the study. An opening of the delaminated section is observed across the width of the stringer over the entire delaminated section as shown in Figure 9b. The same deformation was also observed for the local insert model shown in Figures 9c where the stinger foot and adjacent panel skin were meshed uniformly with 30 elements across the width of the stringer foot. The same opening is also observed for modeled delamination lengths a= 88.9 mm and 94.9 mm as shown in Figures 10a and b. The detail of the deformed local model for a delamination length a=101.6 mm is shown in Figure 10c for the last analysis increment. The figure reveals that not the entire delaminated section opens under mode I. After initial opening, the section below the web termination closes and the delaminated surfaces contact. This closing is caused by a change in the local buckling pattern, due to stiffness changes caused by the longer delamination. It was observed that the local buckling pattern in the immediate surrounding of the delaminated stringer is very sensitive to the delamination length modeled, which made convergence difficult. For the models representing delamination lengths a=203.2 mm as show in Figure 10d and a=279.4 mm as shown in Figure 10e an opening of the delaminated section is observed for the entire delamination length modeled. Partial closure of the delaminated surfaces which result in local contact is observed for the analysis of the a=355.6 mm delamination as shown in Figure 10f. The observed deformations match the results from a related study where the entire delaminated section of the stringer had been modeled with solid elements [12].

4.2 Calculation of Mixed-Mode Strain Energy Release Rates and Failure Indices

The virtual crack closure technique (VCCT) – discussed earlier - was used to calculate the mode contributions G_I, G_{II} and G_{III} the total energy release rate G_T=G_I+G_{II}+G_{III}, as well as the mixed mode ratios G_S/G_T along the delamination front across the width b of the stringer for all delamination lengths modeled. Here G_S denotes the sum of the in-plane shearing components G_{II}+G_{III}. For two-dimensional analyses, where G_{III}=0, this definition is equal to the commonly used definition of the mixed mode ratio, G_{II}/G_T. For three-dimensional analysis, which also yields results for the scissoring mode G_{III}, the modified definition of G_S is introduced since a mixed-mode failure criterion, which accounts for all three modes is currently not available.

For each nodal point along the delamination front the critical energy release rate G_c was calculated from the mixed mode failure criterion for IM7/8552 graphite/epoxy (Figure 3)

$$G_c = 207.7 + 1126.8 \cdot \left(\frac{G_S}{G_T} \right)^{4.46} . \qquad (2)$$

for the computed mixed-mode ratio G_S/G_T at each point. Subsequently the failure index G_T/G_c was determined with the assumption that delamination propagation occurs for

$$\frac{G_T}{G_c} \geq 1. \tag{3}$$

For all delamination lengths modeled, the computed failure indices were calculated for every fifth load increment plus the final increment and plotted versus the dimensionless coordinate s across the width of the stringer b

$$s(y) = \frac{y - y_0}{b}; \quad 0.0 \leq s \leq 1.0. \tag{4}$$

At the left edge of the stringer the nodal point coordinates are equal to $y=y_0$ which yields s=0.0 and the right edge nodal point coordinates are equal to $y=y_b$ which results in s=1.0 as depicted in Figure 7.

For all delamination lengths modeled the calculated failure indices are shown in Figures 11 to 17. Since it was difficult to get corresponding results at the same load increment for different models, failure indices were calculated and plotted for the last analysis increment after the entire external displacement $u=v$=6.35 mm had been applied. The calculated failure indices for delamination length a=81.9 mm are shown in Figure 11 for different models used. The distribution obtained from the inserts shown in Figure 9b and c is plotted together with the result obtained from the model of a related study [12] shown in Figure 1b. The failure index peaked at the edges (s=0.0 and s=1.0) with an additional peak around the center (s~0.5) underneath the stringer. The values in the center were higher for the model with 30 elements across the width. This can be explained since the mesh is finer in the center and is able to describe the failure index distribution in more detail. Overall, the results were in good agreement and showed that the computation of the failure index was insensitive to minor changes in the model.

The failure indices computed for delamination length a=88.9, 94.6, 101.6, 203.2, 279.4 and 355.6 mm are shown in Figures 12 to 17 for different models used. The distributions obtained from the inserts shown in Figure 10 are plotted together with the result obtained from the model of a related study [12]. For delamination lengths a=88.9 mm and 94.6 mm the results were in good agreement as shown in Figures 12 and 13.

For longer delaminations a=101.6, 203.2, 279.4 and 355.6 mm the distributions across the width obtained from the short inserts follow the same trend as the results from the original study however differences in the center and near the edges become visible. The differences may be caused by the local shell to solid coupling. For the original models shown in Figures 1b and c the local 3D insert models are connected to many shell nodes and closely follow the deformation of the global shell model. Away from the stinger termination the center stringer is modeled with a coarse shell mesh as shown in Figure 7a and therefore fewer shell nodes connect to the significantly shorter local insert as shown e.g. in Figure 10e. The deformation of the shorter insert may therefore not follow the deformed global shell model as well as the models which are connected to more shell nodes.

For the models used for delamination length a=101.6 mm and 203.2 mm the mesh of the stringer web and foot and panel skin adjacent to the insert was manually refined as shown in Figures 10c and d. The modified mesh yielded failure indices across the width which were in

better agreement with the reference results [12] as shown in Figures 14 and 15. It is assumed that additional local refinement of the shell models near the flange edges would further improve the results. With respect to the distributions shown in Figures 16 and 17 local refinements of the stringer shell model are also expected to yield better agreements with the reference results [12] for delamination lengths a=279.4 and 355.6 mm. Additional analysis will be required to validate this assumption.

5. SUMMARY AND CONCLUDING REMARKS

The skin/stringer separation of a graphite/epoxy composite panel reinforced with three stringers and subjected to pure shear loading was studied using computational fracture analysis. The shear loading causes the panel to buckle and the resulting out-of-plane deformation initiates skin/stringer separation at the location of an embedded defect. The panel and surrounding load fixture were modeled with shell elements.

A small section of the stringer foot and the panel in the vicinity of the delamination front were modeled with a local 3D solid model. A total of seven delamination lengths between 81.9 and 355.6 mm were modeled. Across the width of the stringer foot the mixed-mode strain energy release rates were calculated using the virtual crack closure technique. A failure index was calculated by correlating the results with the mixed-mode failure criterion of the graphite/epoxy material. Computed failure indices were compared to corresponding results from a related study where the entire delaminated section of the stiffener foot had been modeled with solid elements.

Computed failure indices were in good agreement with results from models where the entire delaminated section of the stiffener foot had been modeled with solid elements. Changing the model, which had a coarse mesh in the center and a fine mesh near the edges to a uniform mesh across the entire width of the stiffener foot, had a negligible influence on the results. The results showed that the failure indices were fairly insensitive to minor changes in the model. It was observed that the shell-to-solid connection influenced the computed failure indices. Local refinement of the shell model across the stringer foot and web improved the results. It is assumed that additional local refinement of the shell model near the flange edges would further improve the results. Additional analysis will be required to substantiate this assumption.

Overall the study confirmed that the section modeled locally did not have to include the entire delaminated section. The use of a smaller local inserts reduced model size without compromising the computed failure indices.

ACKNOWLEDGEMENTS.

This research was supported by The Boeing Company and the Aviation Applied Technology Directorate under Technology Investment Agreement No. DAAH10-02-2-0001 as part of the Survivable, Affordable, Repairable, Airframe Program (SARAP).

The authors gratefully acknowledge Dr. Dale Berry of ABAQUS® Central for providing guidance and help when problems with ABAQUS® Standard were encountered during the analyses.

REFERENCES

[1] I. S. Raju, R. Sistla, and T. Krishnamurthy, "Fracture Mechanics Analyses for Skin-Stiffener Debonding," *Eng. Fracture Mech.*, vol. 54, pp. 371-385, 1996.

[2] E. H. Glaessgen, I. S. Raju, and C. C. Poe, "Fracture Mechanics Analysis of Stitched Stiffener-Skin Debonding," in *The 39th AIAA/ASME/ASCE/AHS/ASC Structures, Structural Dynamics and Materials Conference, Long Beach, California, AIAA 98-2022, April 20-23*, 1998.

[3] B. G. Falzon, G. A. O. Davies, and E. Greenhalgh, "Failure of thick-skinned stiffener runout sections loaded in uniaxial compression," *Composite Structures*, vol. 53, pp. 223-233, 2001.

[4] J. W. H. Yap, M. L. Scott, R. S. Thomson, and D. Hachenberg, "The analysis of skin-to-stiffener debonding in composite aerospace structures," *Composite Structures*, vol. 57, pp. 425-435, 2002.

[5] P. J. Minguet, M. J. Fedro, T. K. O'Brien, R. H. Martin, and L. B. Ilcewicz, "Development of a Structural Test Simulating Pressure Pillowing Effects in Bonded Skin/Stringer/Frame Configuration," in *Proceedings of the Fourth NASA/DoD Advanced Composite Technology Conference, Salt Lake City, Utah*, 1993.

[6] P. J. Minguet and T. K. O'Brien, "Analysis of Composite Skin/Stringer Bond Failures Using a Strain Energy Release Rate Approach," in *The Tenth International Conference on Composite Materials*, vol. I, A. Poursartip and K. Street, Eds., 1995, pp. 245-252.

[7] P. J. Minguet and T. K. O'Brien, "Analysis of Test Methods for Characterizing Skin/Stringer Debonding Failures in Reinforced Composite Panels," in *Composite Materials: Testing and Design (Twelfth Volume), ASTM STP 1274*, 1996, pp. 105-124.

[8] P. J. Minguet, "Analysis of the Strength of the Interface Between Frame and Skin in a Bonded Composite Fuselage Panel," in *The 38rd AIAA/ASME/ASCE/AHS/ASC Structures, Structural Dynamics and Materials Conference*, Kissimmee, Florida, 1997, pp. 2783-2790.

[9] R. Krueger, M. K. Cvitkovich, T. K. O'Brien, and P. J. Minguet, "Testing and Analysis of Composite Skin/Stringer Debonding Under Multi-Axial Loading," *Journal of Composite Materials*, vol. 34, pp. 1263-1300, 2000.

[10] R. Krueger, I. L. Paris, T. K. O'Brien, and P. J. Minguet, "Fatigue Life Methodology for Bonded Composite Skin/Stringer Configurations," *Journal of Composites Technology and Research*, vol. 24, pp. 56-79, 2002.

[11] T. K. O'Brien, "Fracture Mechanics of Composite Delamination," in *ASM Handbook, Volume 21, Composites*: ASM International, 2001, pp. 241-245.

[12] R. Krueger and P. J. Minguet, "Skin-Stiffener Debond Prediction Based on Computational Fracture Analysis," Hampton, VA, NIA Report No. 2005-06, 2005.

[13] R. H. Martin, "Incorporating interlaminar fracture mechanics into design," in *International Conference on Designing Cost-Effective Composites*: IMechE Conference Transactions, London, U.K., 1998, pp. 83-92.

[14] "ASTM D 5528-94a, Standard Test Method for Mode I Interlaminar Fracture Toughness of Unidirectional Fiber-Reinforced Polymer Matrix Composites," in *Annual Book of ASTM Standards*, vol. 15.03: American Society for Testing and Materials, 2000.

[15] "ASTM D 6671-01, Standard Test Method for Mixed Mode I-Mode II Interlaminar Fracture Toughness of Unidirectional Fiber Reinforced Polymer Matrix Composites," in

Annual Book of ASTM Standards, vol. 15.03: American Society for Testing and Materials, 2000.

[16] R. H. Martin and B. D. Davidson, "Mode II Fracture Toughness Evaluation Using A Four Point Bend End Notched Flexure Test," *Plastics, Rubber and Composites*, vol. 28, pp. 401-406, 1999.

[17] M. L. Benzeggagh and M. Kenane, "Measurement of mixed-mode delamination fracture toughness of unidirectional glass/epoxy composites with mixed-mode bending apparatus," *Composites Science and Technology*, vol. 56, pp. 439-449, 1996.

[18] R. H. Martin, "Evaluation of the Split Cantilever Beam for Mode III Delamination Testing," in *Composite Materials: Fatigue and Fracture (Third Volume), ASTM STP 1110*, 1991, pp. 243-266.

[19] S. M. Lee, "An Edge Crack Torsion Method for Mode III Delamination Fracture Testing," *J. of Composite Technology and Research.*, pp. 193--201, 1993.

[20] P. Robinson and D. Q. Song, "A new Mode III delamination test for composites," *Advanced Composites Letters*, vol. 1, pp. 160--164, 1992.

[21] J. Li, S. M. Lee, E. W. Lee, and T. K. O'Brien, "Evaluation of the Edge Crack Torsion ECT Test for Mode III Interlaminar Fracture Toughness of Laminated Composites," *Journal of Composites Technology and Research*, vol. 19, pp. 174-183, 1997.

[22] J. G. Ratcliffe, "Characterization of the Edge Crack Torsion (ECT) Test for Mode III Fracture Toughness Measurement of Laminated Composites," NASA/TM-2004-213269 September 2004.

[23] R. Krueger, "Virtual Crack Closure Technique: History, Approach and Applications," *Applied Mechanics Reviews*, vol. 57, pp. 109-143, 2004.

[24] E. F. Rybicki and M. F. Kanninen, "A Finite Element Calculation of Stress Intensity Factors by a Modified Crack Closure Integral," *Eng. Fracture Mech.*, vol. 9, pp. 931-938, 1977.

[25] E. H. Glaessgen, W. T. Riddell, and I. S. Raju, "Effect of Shear Deformation and Continuity on Delamination Modeling with Plate Elements," in *The 39rd AIAA/ASME/ASCE/AHS/ASC Structures, Structural Dynamics and Materials Conference*, Long Beach, California, 1998.

[26] E. H. Glaessgen, W. T. Riddell, and I. S. Raju, "Nodal Constraint, Shear Deformation and Continuity Effects Related to the Modeling of Debonding of Laminates, Using Plate Elements," *CMES*, vol. 3, pp. 103-116, 2002.

[27] J. T. Wang and I. S. Raju, "Strain energy release rate formulae for skin-stiffener debond modeled with plate elements," *Eng. Fracture Mech.*, vol. 54, pp. 211-228, 1996.

[28] R. Krueger and T. K. O'Brien, "A Shell/3D Modeling Technique for the Analysis of Delaminated Composite Laminates," NASA/TM-2000-210287, ARL-TR-2207, 2000.

[29] R. Krueger and T. K. O'Brien, "A Shell/3D Modeling Technique for the Analysis of Delaminated Composite Laminates," *Composites Part A: Applied Science and Manufacturing*, vol. 32, pp. 25-44, 2001.

[30] R. Krueger and P. J. Minguet, "Analysis of Composite Skin-Stiffener Debond Specimens Using a Shell/3D Modeling Technique and Submodeling," Hampton, VA, NIA Report No. 2004-04, NASA/CR-2004-212684, 2004.

[31] R. Krueger and P. J. Minguet, "Analysis of Composite Skin-stiffener Debond Specimens Using Volume Elements and a Shell/3D Modeling Technique," NASA/CR-2002-211947, ICASE Report No. 2002-38, October 2002.

Table 1.

Material Properties

IM7/8552 Unidirectional Graphite/Epoxy Prepreg		
E_{11} = 150.0 GPa	E_{22} = 10.7 GPa	E_{33} = 10.7 GPa
ν_{12} = 0.33	ν_{13} = 0.33	ν_{23} = 0.45
G_{12} = 4.8 GPa	G_{13} = 4.8 GPa	G_{23} = 3.4 GPa
IM7/8552 Graphite/Epoxy Plain Weave Fabric		
E_{11} = 73.1 GPa	E_{22} = 73.1 GPa	E_{33} = 10.6 GPa
ν_{12} = 0.04	ν_{13} = 0.35	ν_{23} = 0.35
G_{12} = 4.8 GPa	G_{13} = 4.1 GPa	G_{23} = 4.1 GPa
8552 Resin		
E = 4.67 GPa	ν = 0.37	(assumed isotropic)
Steel		
E = 206.8 GPa	ν = 0.33	(assumed isotropic)

The material properties are given with reference to the ply coordinate axes where index 11 denotes the ply principal axis that coincides with the direction of maximum in-plane Young's modulus (fiber direction). Index 22 denotes the direction transverse to the fiber in the plane of the lamina and index 33 the direction perpendicular to the plane of the lamina.

Table 2.

Size of Solid Finite Element Insert Model

Delamination length a* in mm	Local 3D insert, reference [12]		Local 3D insert	
	length c* in mm	Number of solid elements C3D8I	length c* in mm	Number of solid elements C3D8I
81.9	Short local 3D insert[+] c=113.7 mm	*8320*	38.1	*4992*
88.9	Short local 3D insert[+] c=113.7 mm	*7488*	39.2	*5200*
94.6	Short local 3D insert[+] c=113.7 mm	*8112*	31.8	*4576*
101.6	Short local 3D insert[+] c=113.7 mm	*8320*	23.8	*4160*
127.0	Long local 3D insert[++] c=431.2 mm	11440	-	
203.2	Long local 3D insert[++] c=431.2 mm	*12480*	63.5	*6656*
279.4	Long local 3D insert[++] c=431.2 mm	*13728*	63.5	*6448*
355.6	Long local 3D insert[++] c=431.2 mm	*14768*	55.6	*6240*

*Delamination length a and length of local 3D insert c as defined in Figure 7b

[+] Short local 3D insert as shown in Figure 1b

[++] Long local 3D insert as shown in Figure 1c

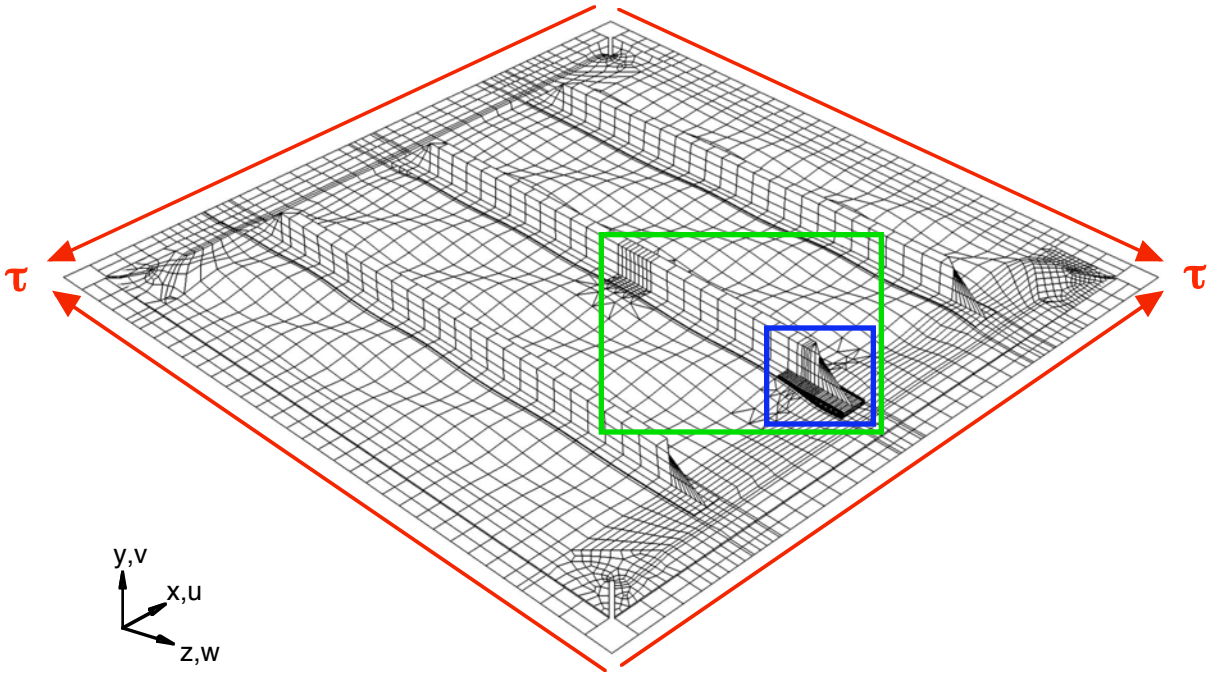

a. *Deformed three-stringer panel under shear loading*

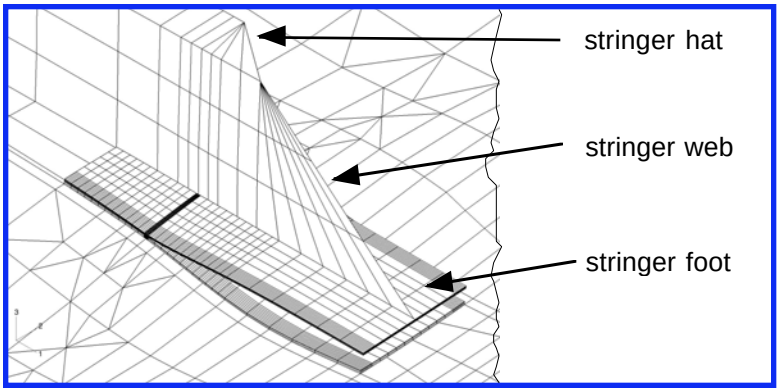

b. *Short local 3D insert near stringer termination with a=81.9 mm delamination length*

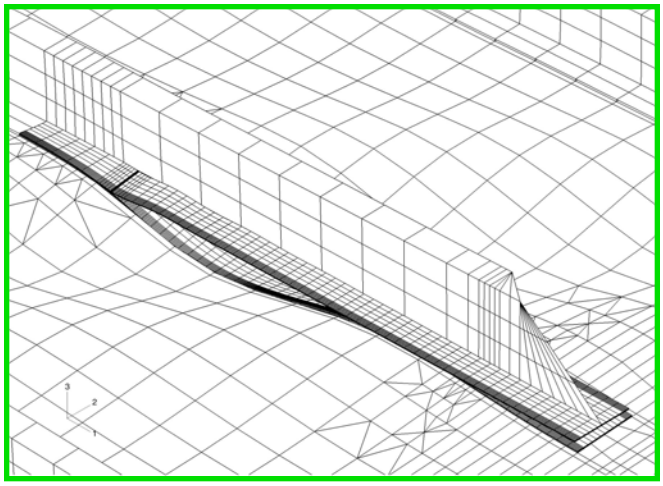

c. *Long local 3D insert with a=355.6 mm delamination length*

Figure 1: *Stringer Stiffened Panel [12]*

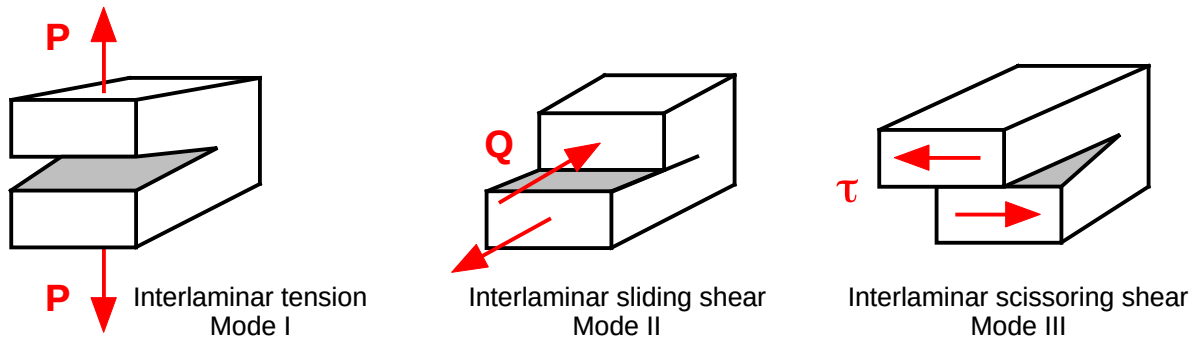

Figure 2: *Fracture Modes.*

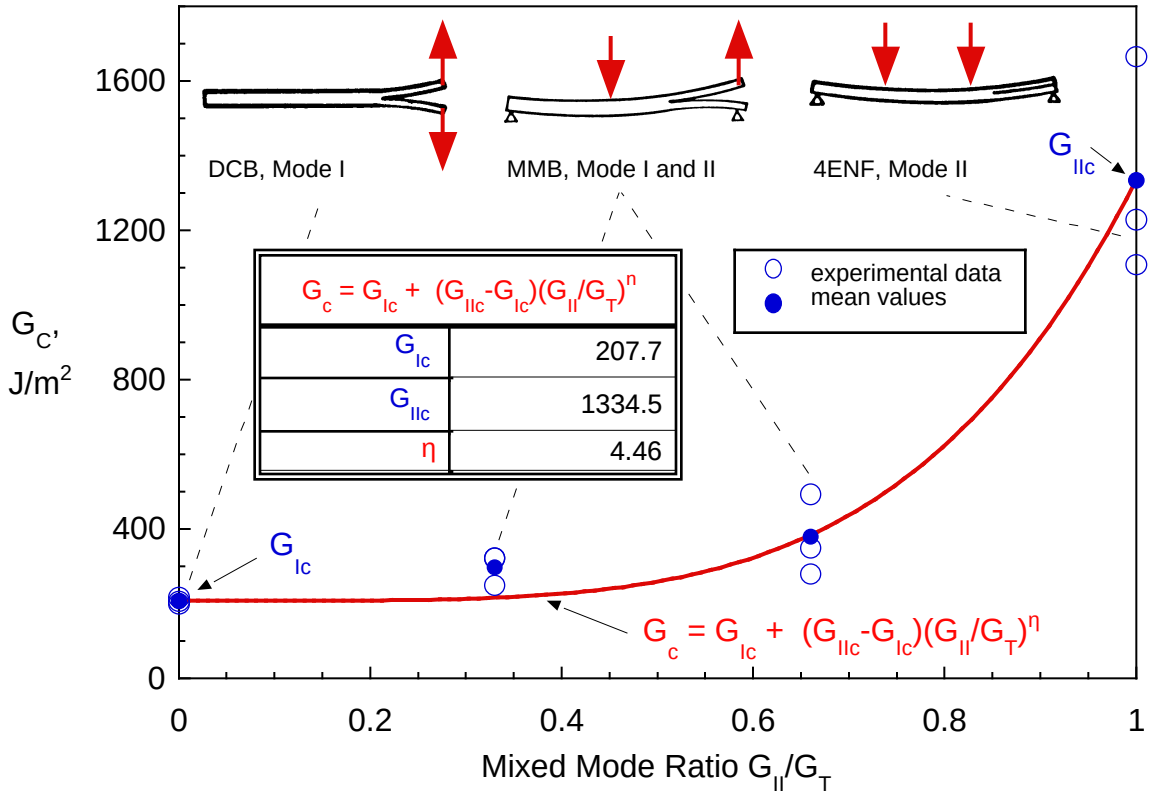

Figure 3: *Mixed-mode fracture criterion for IM7/8552 .*

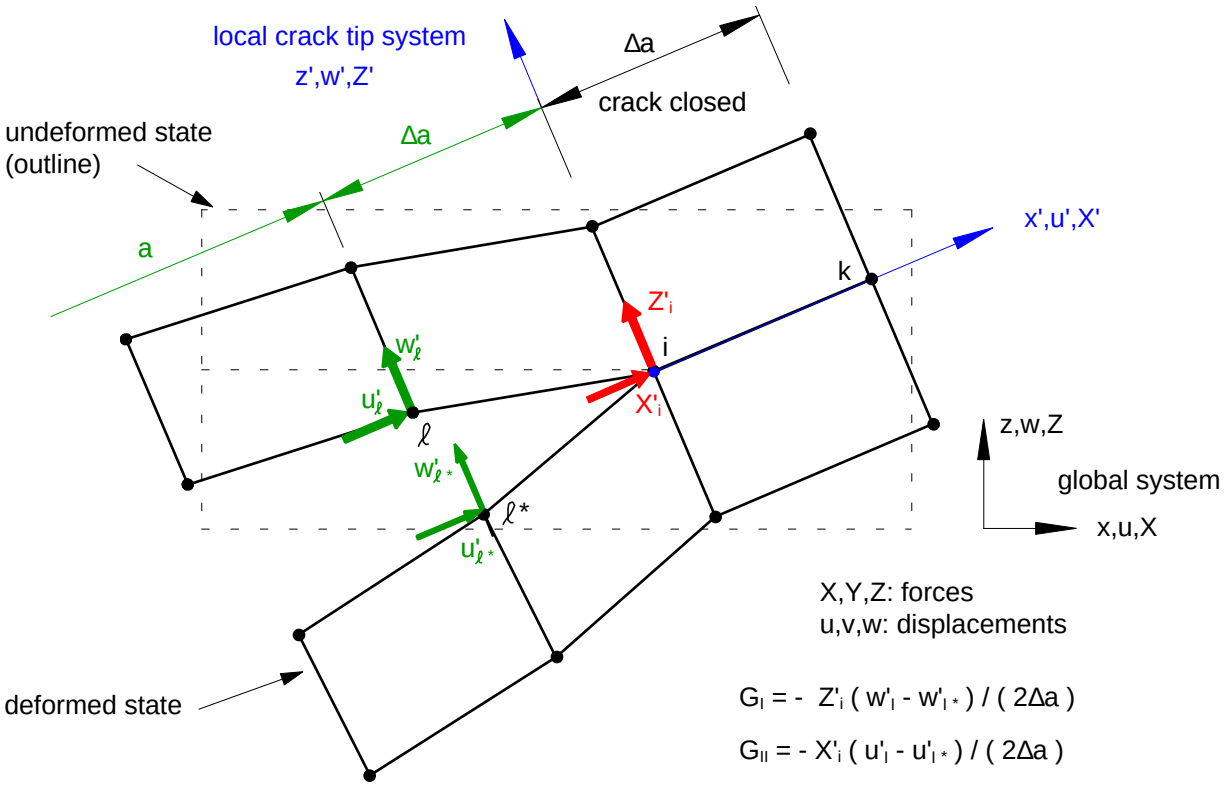

(a): *VCCT for geometrically nonlinear analysis.*

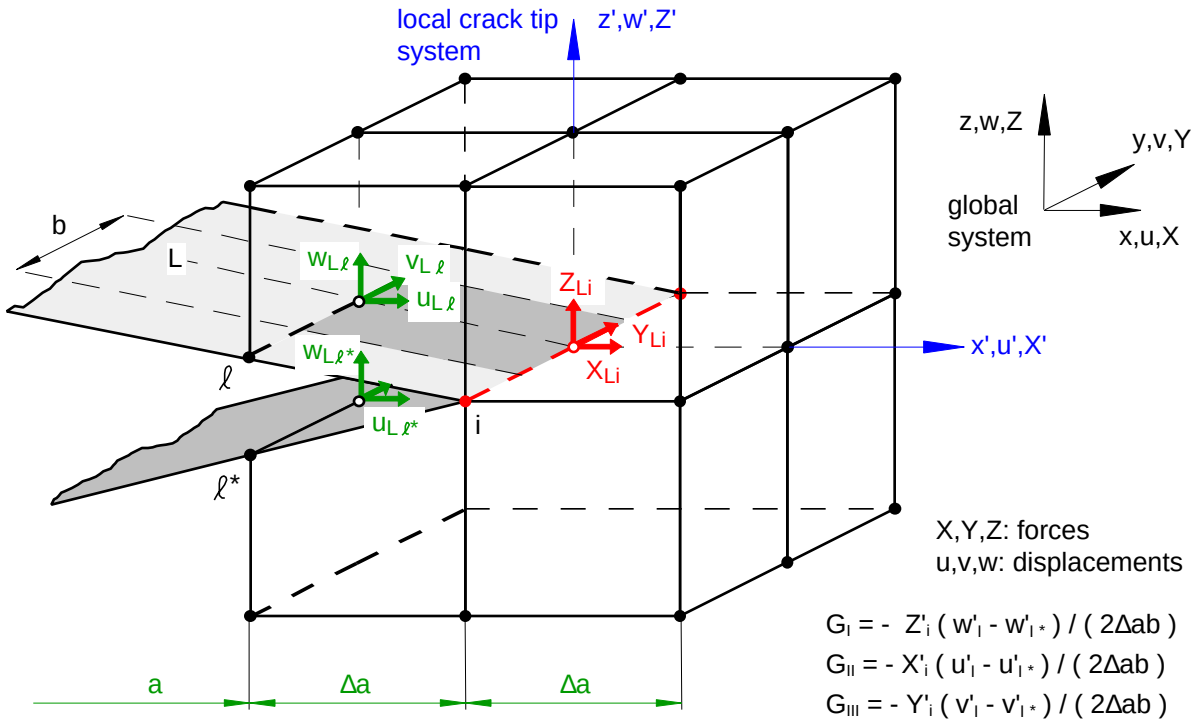

(b). *VCCT for eight noded solid elements.*

Figure 4: *Virtual Crack Closure Technique (VCCT).*

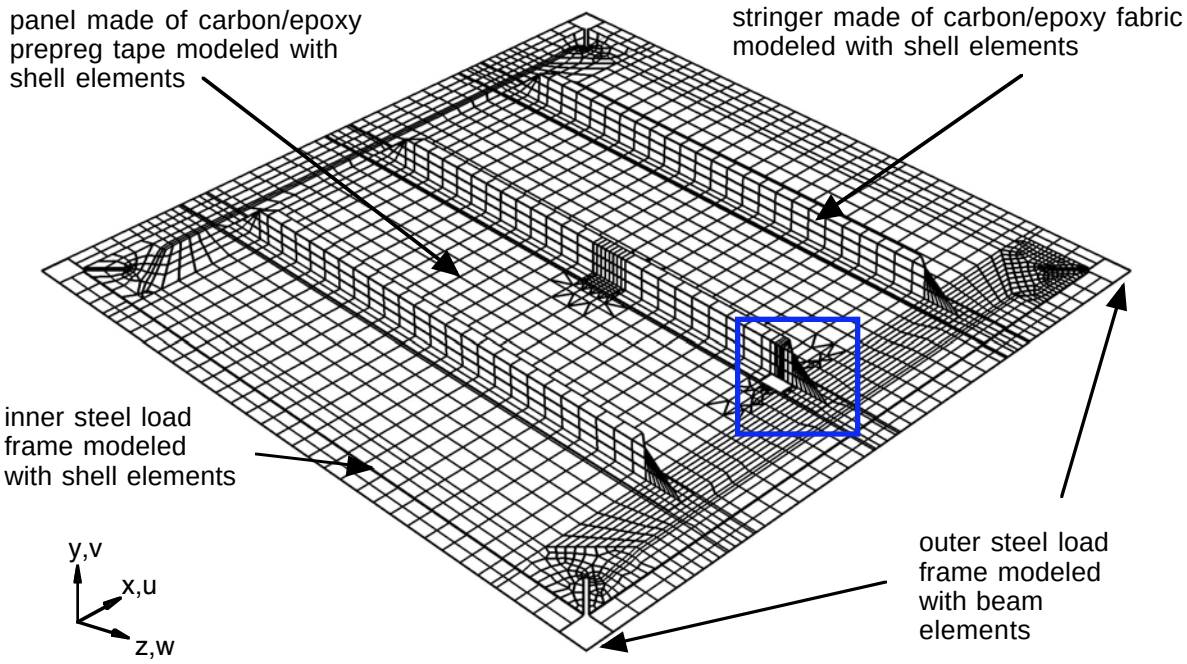

a. *Composite panel and load frame components*

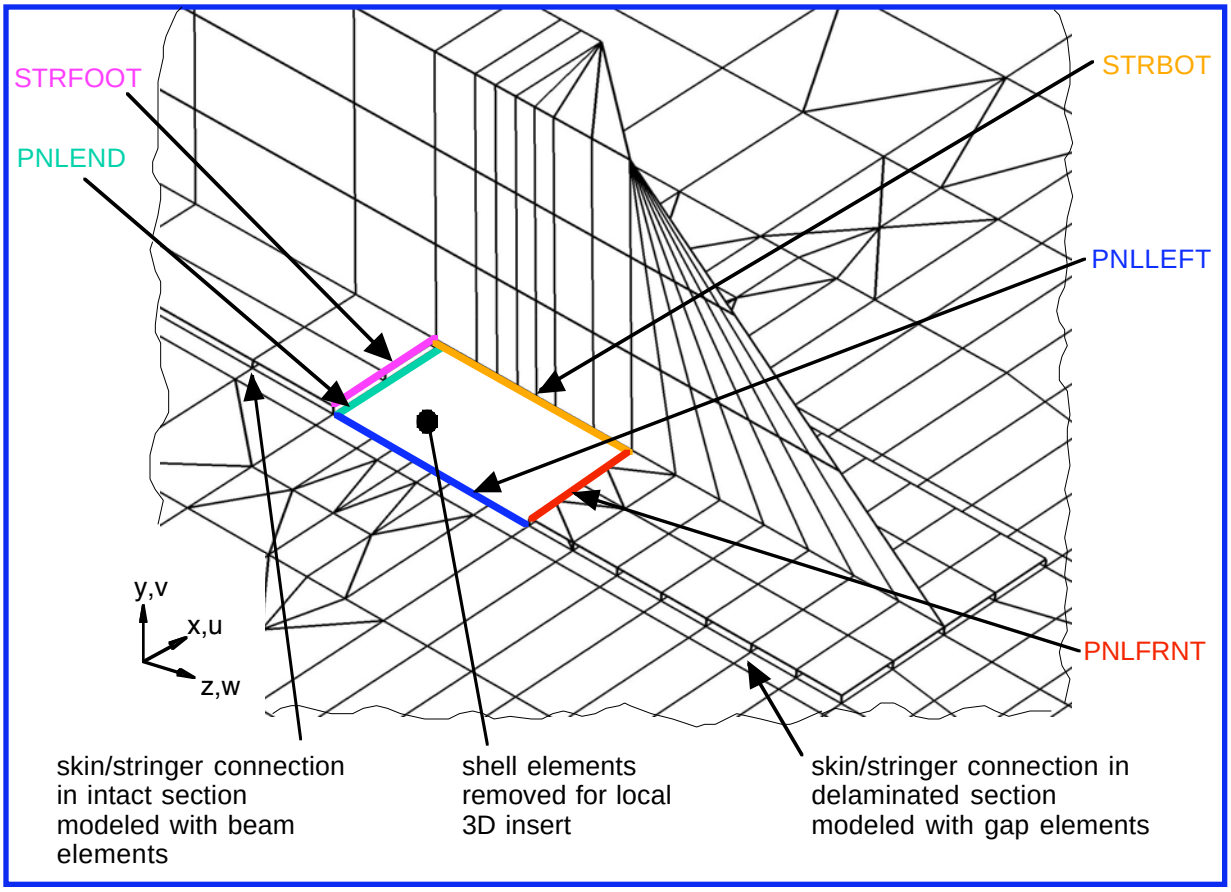

b. *Detail of global shell model with edges for shell to solid coupling*

Figure 5: *Global shell model of stringer stiffened panel*

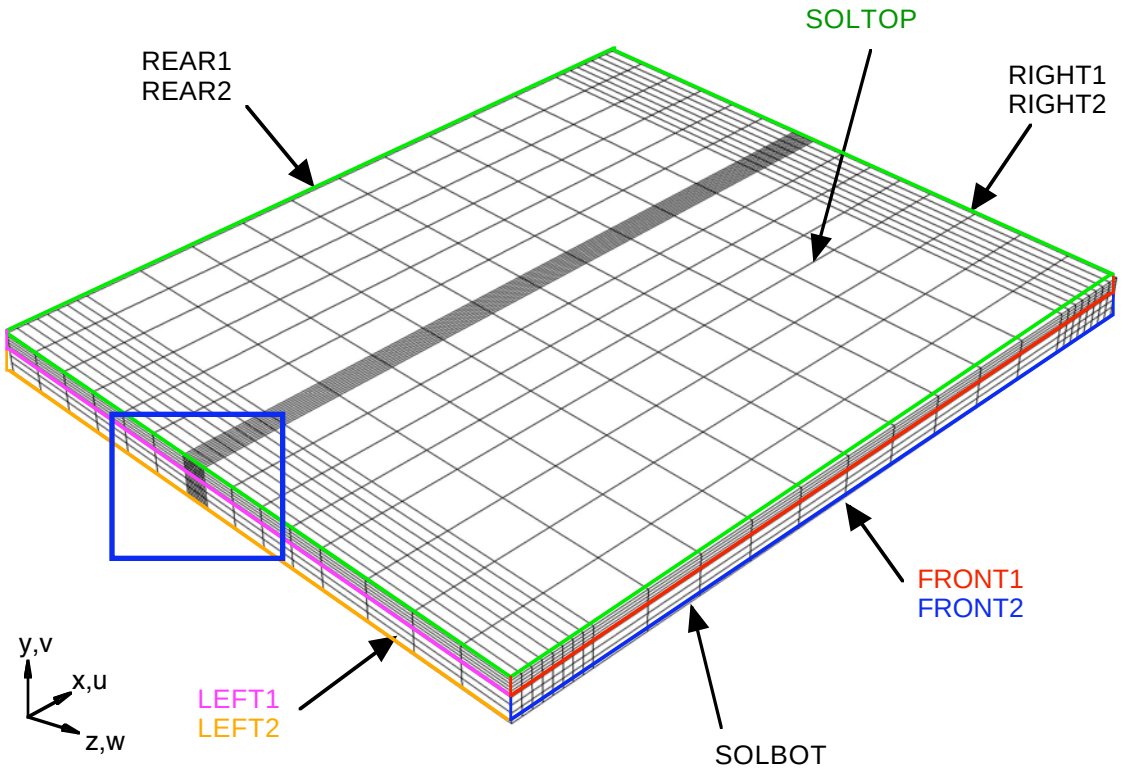

a. *Local 3D insert model and surfaces for shell to solid coupling*

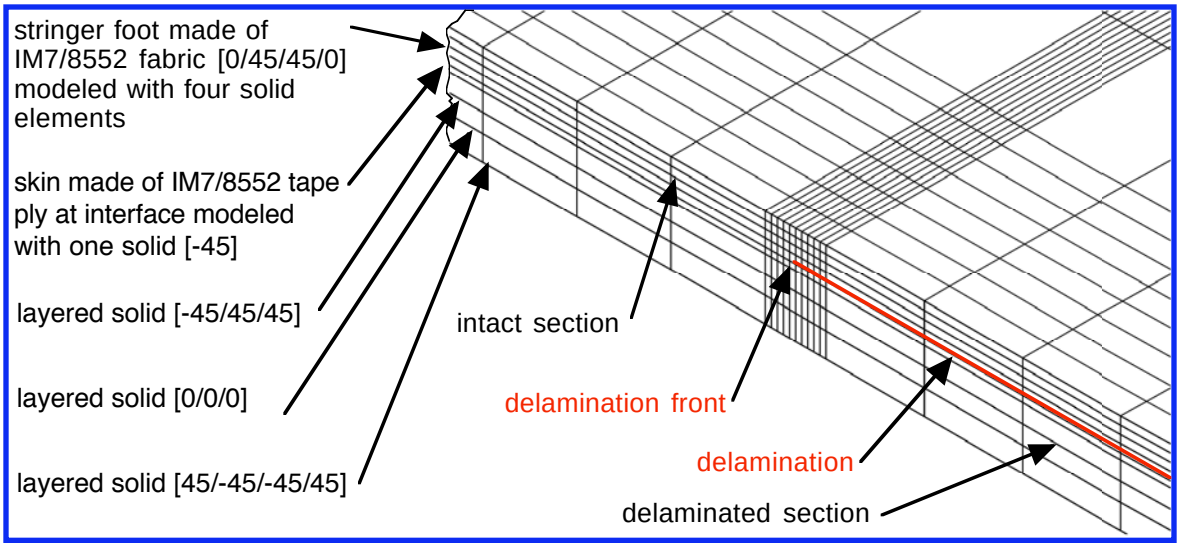

b. *Detail of local 3D insert model around delamination front*

Figure 6: *Local insert model*

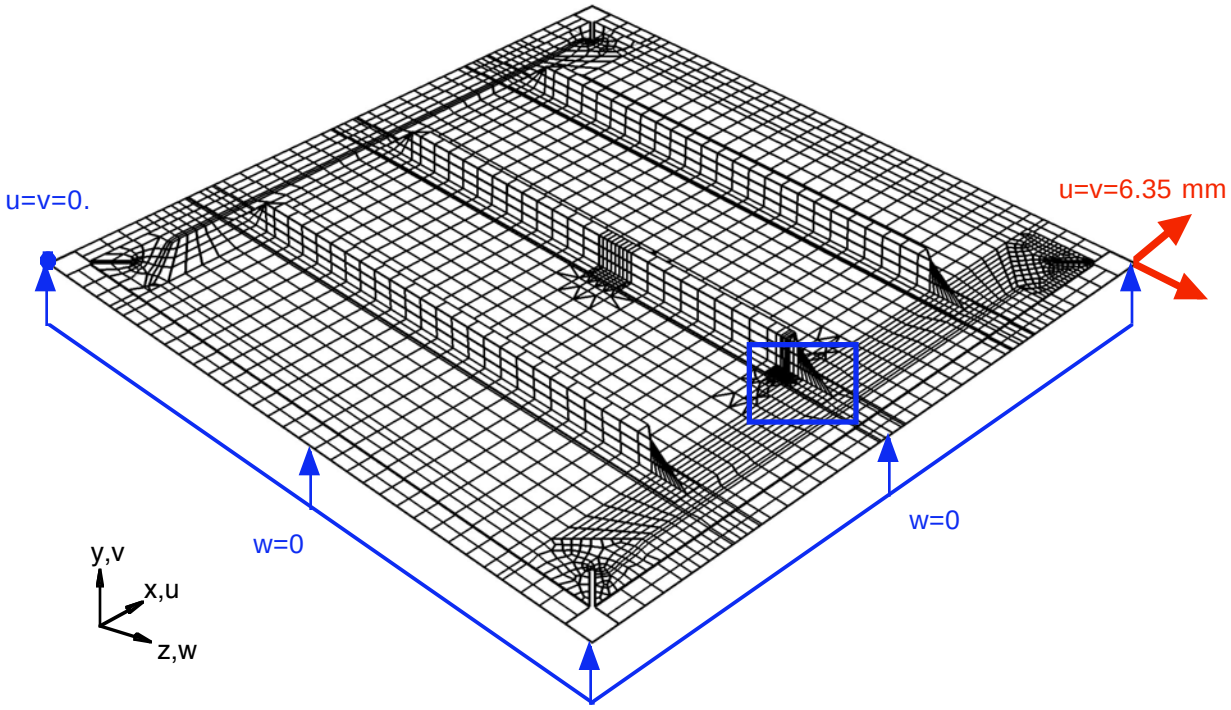

a. *Finite element model with load and boundary conditions.*

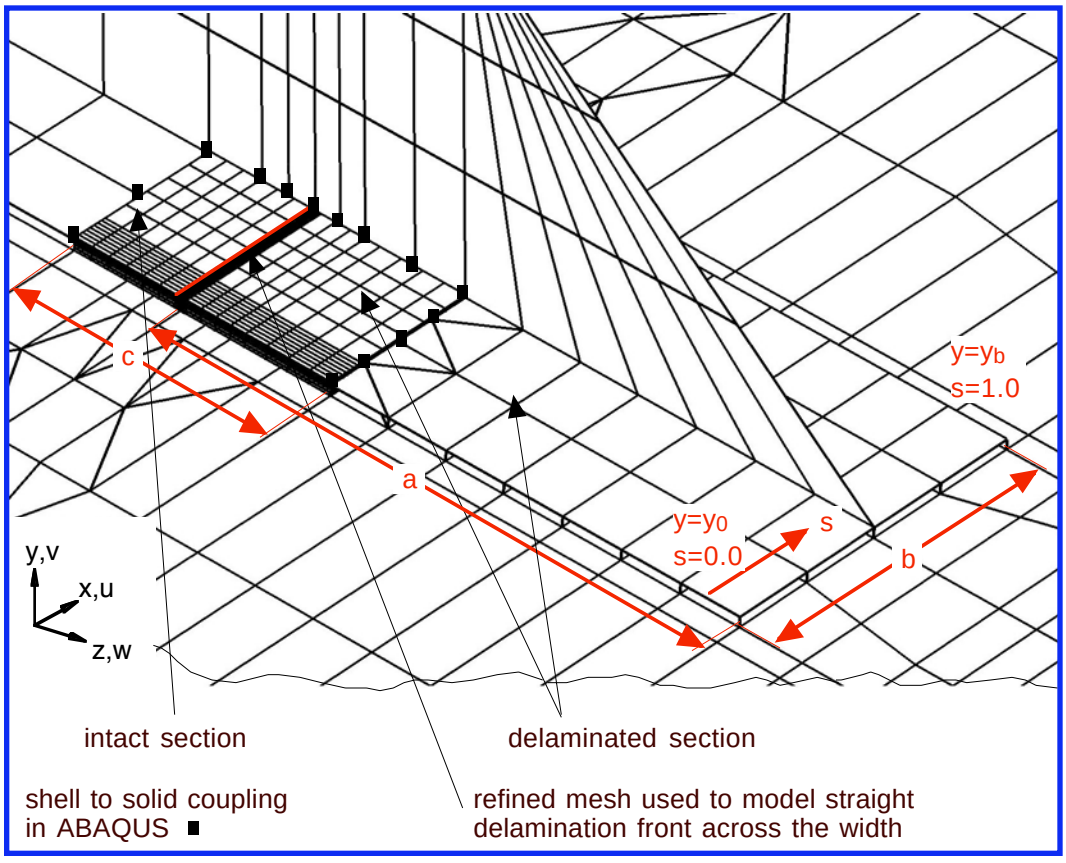

b. *Detail of center stringer with local 3D insert*

Figure 7: *Global shell/local 3D model of stiffened panel*

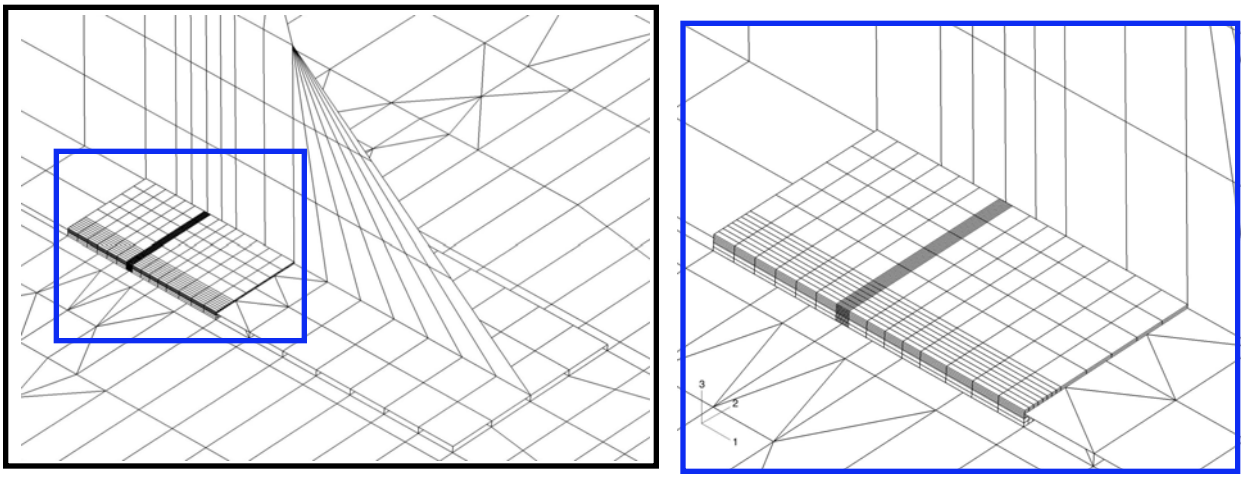

a. *Finite element model of local 3D insert for a=81.9 mm delamination length*

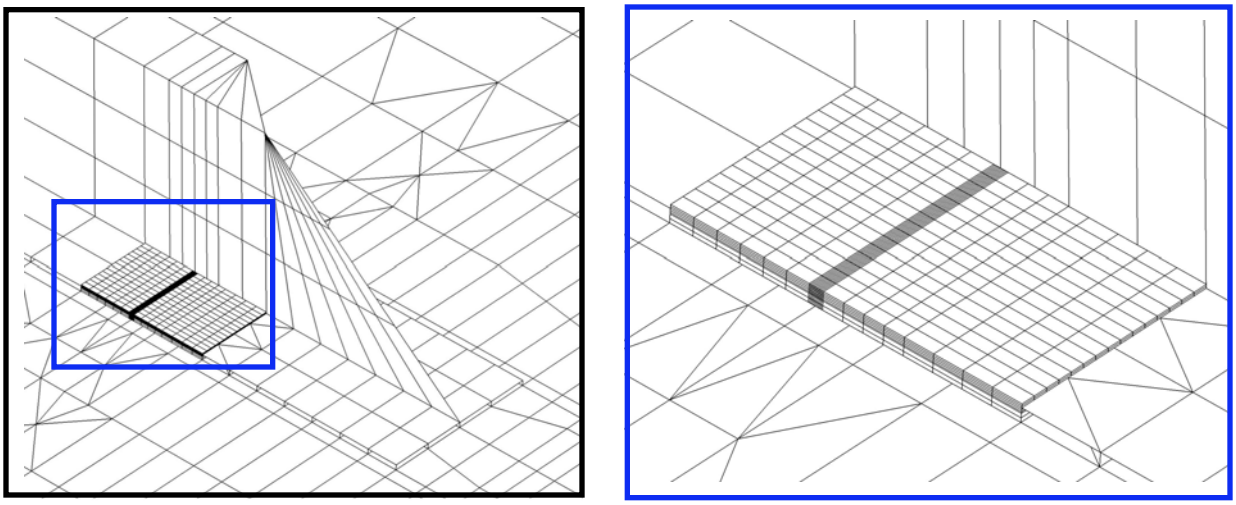

b. *Local 3D insert for a=81.9 mm delamination length with uniform mesh*

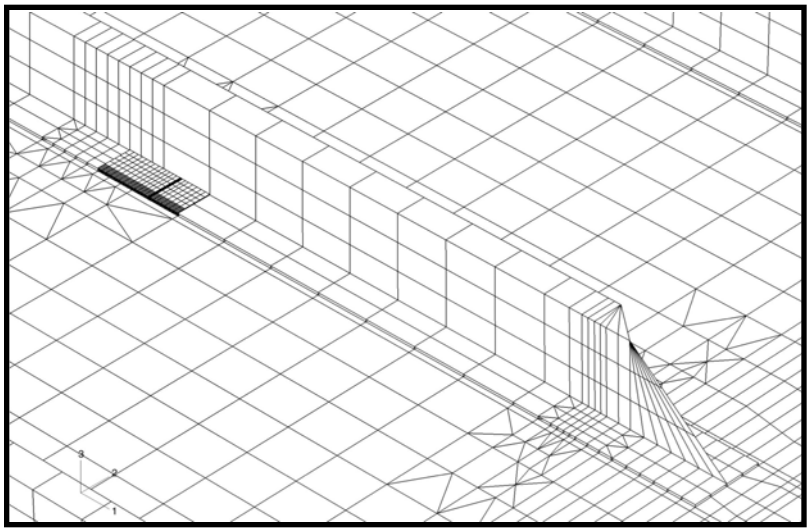

c. *Finite element model of local 3D insert for a=355.6 mm delamination length*

Figure 8: *Finite element models for different delamination lengths*

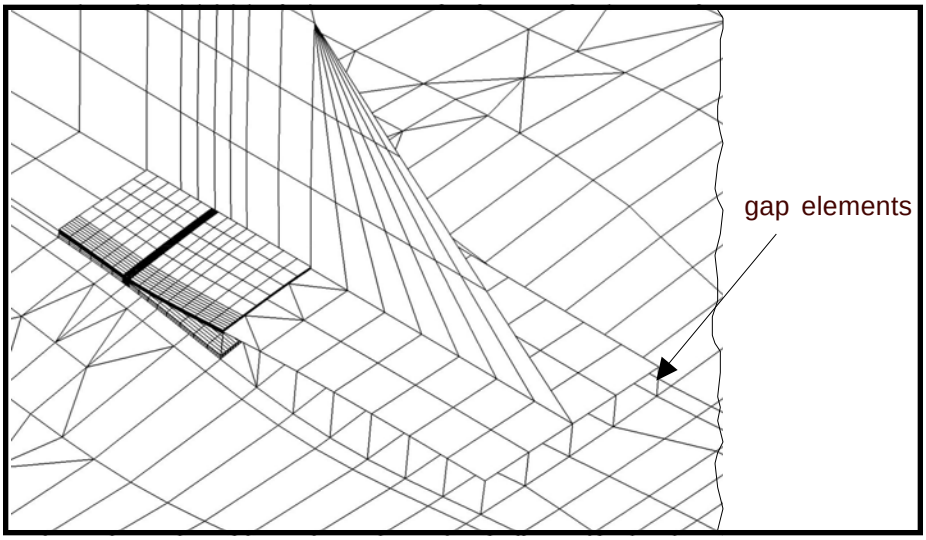

a. *Deformed local 3D insert model with visible gap elements*

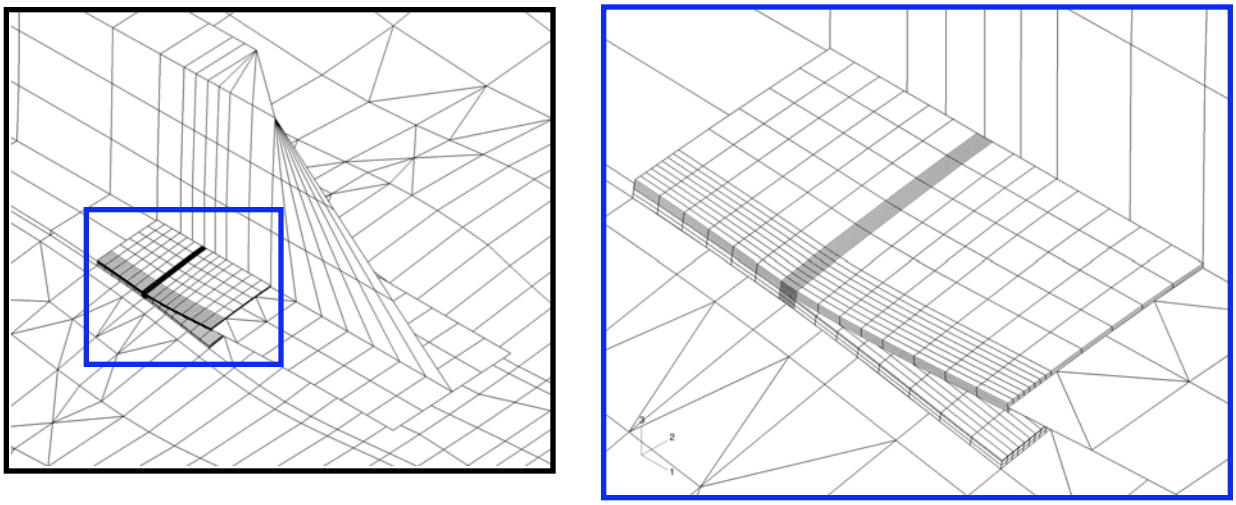

b. *Deformed local 3D insert model with refined mesh at the edge*

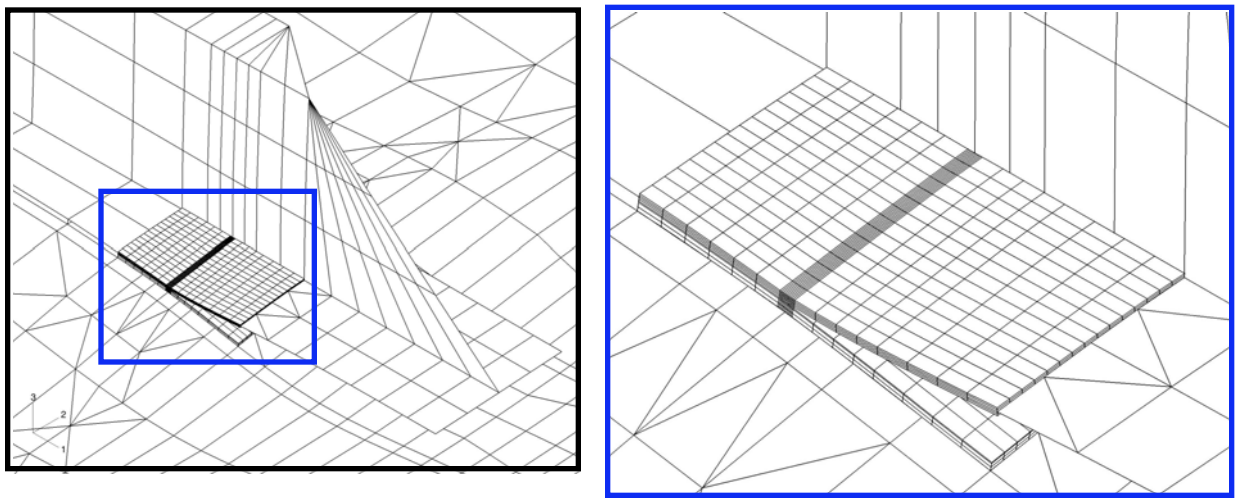

c. *Deformed local 3D insert with uniform mesh across the width*

Figure 9: *Finite element model of local 3D insert for a=81.9 mm delamination length*

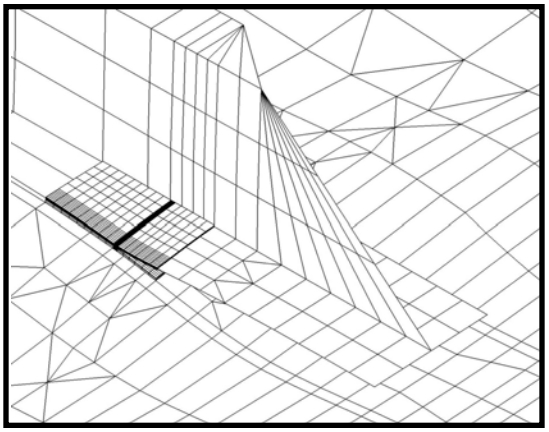

a. *Local 3D insert for a=88.9 mm*

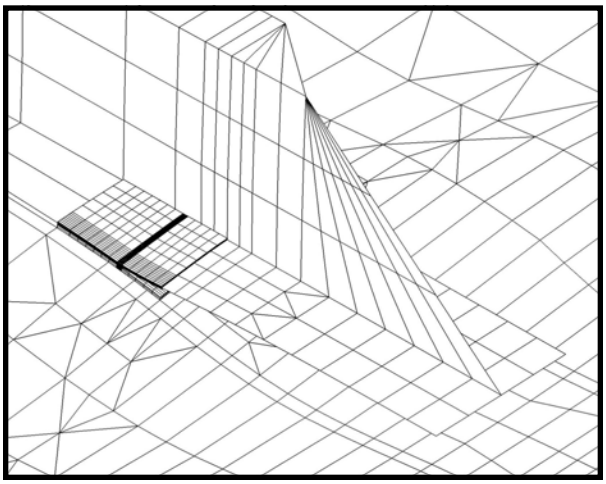

b. *Local 3D insert for a=94.6 mm*

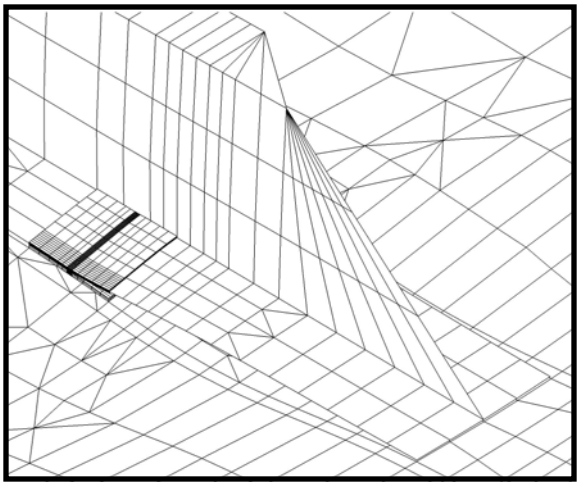

c. *Local 3D insert for a=101.6 mm*

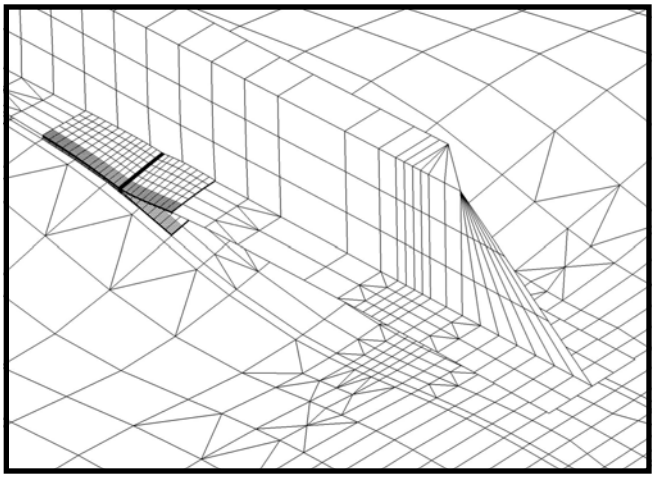

d. *Local 3D insert for a=203.2 mm*

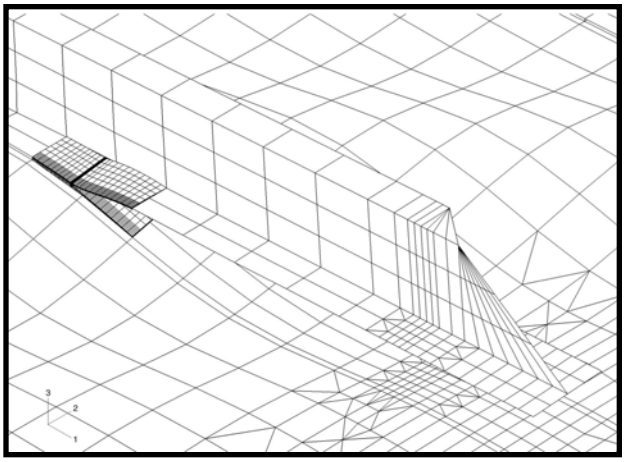

e. *Local 3D insert for a=279.4 mm*

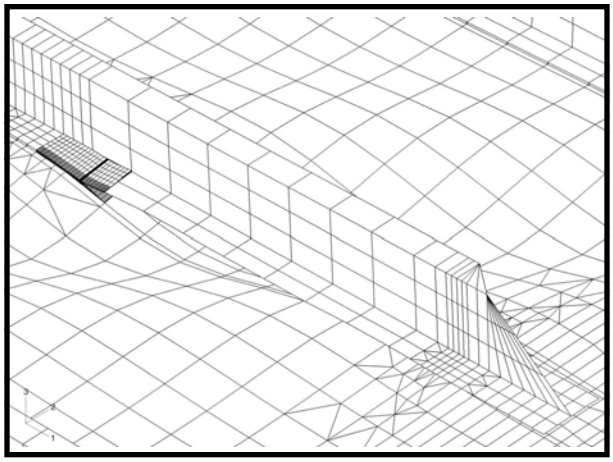

f. *Local 3D insert for a=355.6 mm*

Figure 10: *Deformed center stringer with local 3D inserts for different delamination length a*

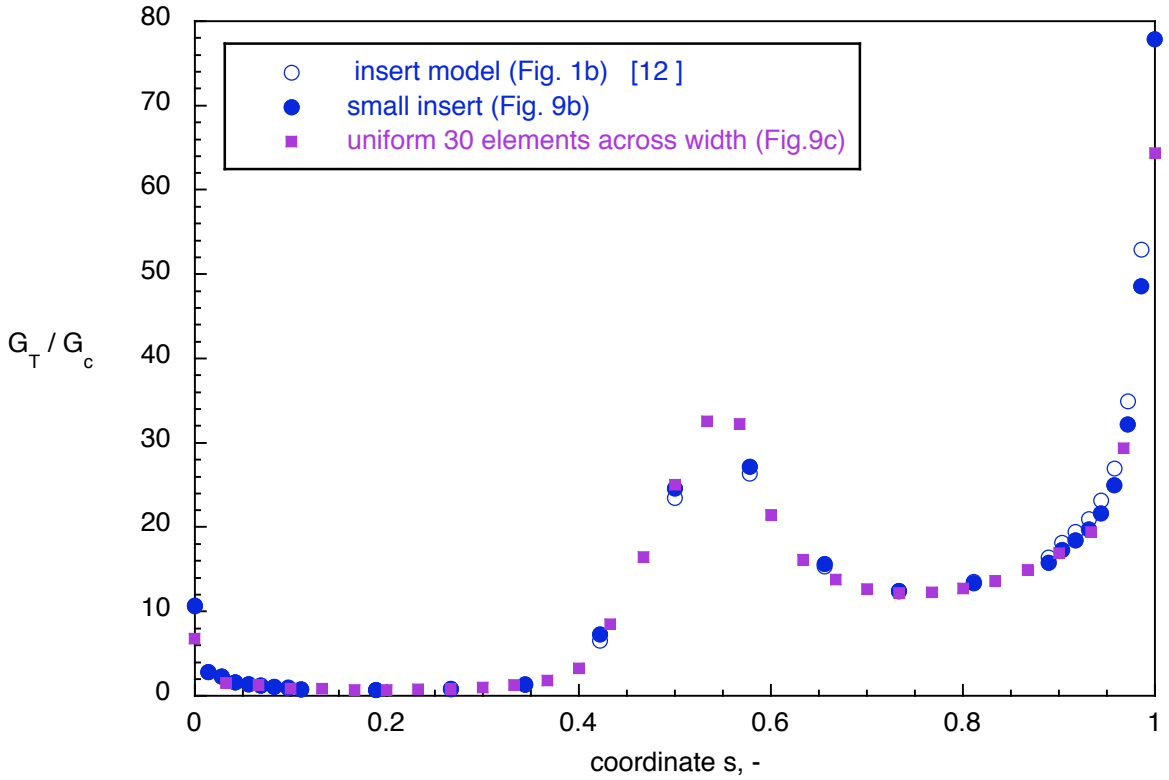

Figure 11. *Computed energy release rate across the width of the stringer obtained from different models for a=81.9 mm*

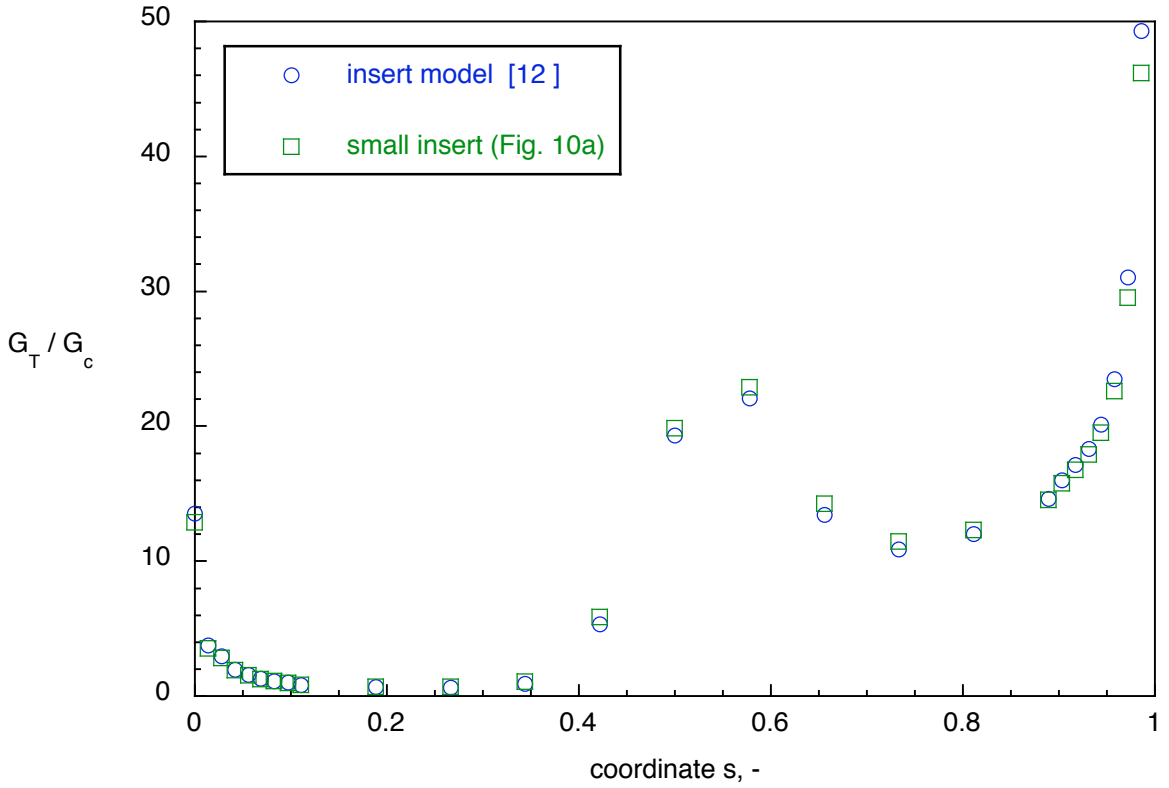

Figure 12. *Computed energy release rate across the width of the stringer for a= 88.9 mm*

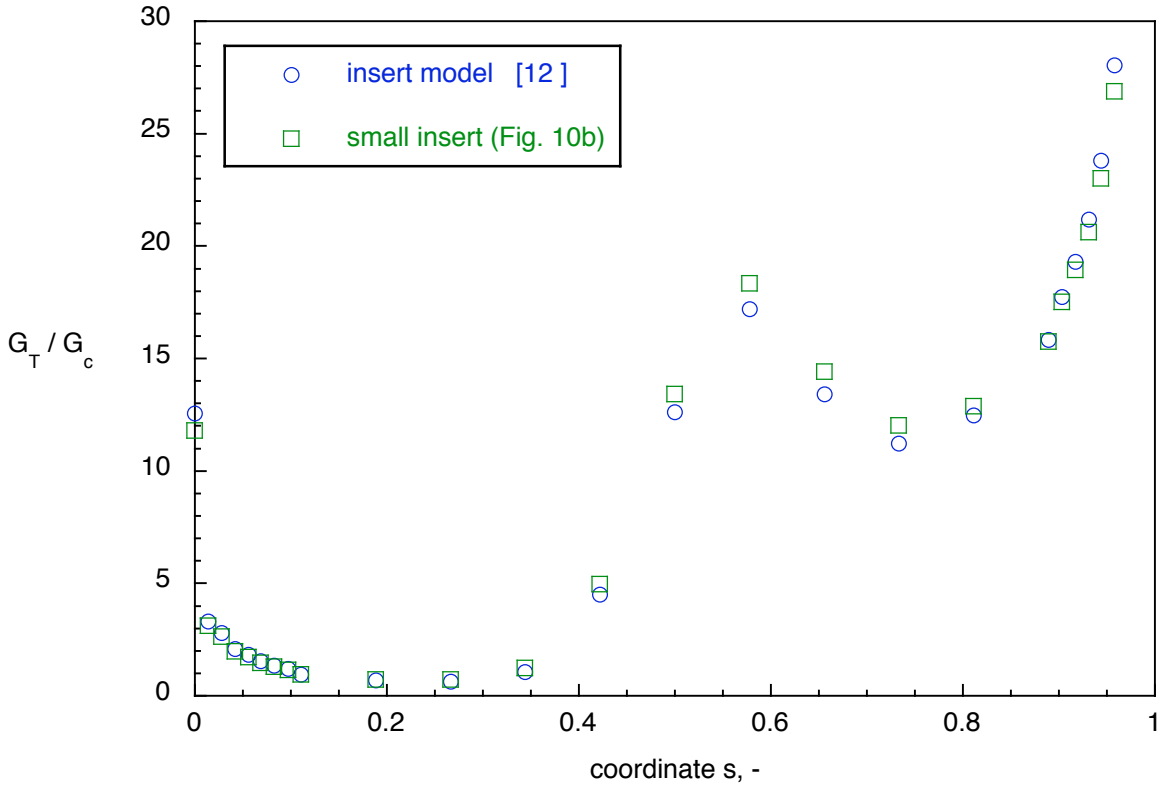

Figure 13. *Computed energy release rate across the width of the stringer for a= 94.6 mm*

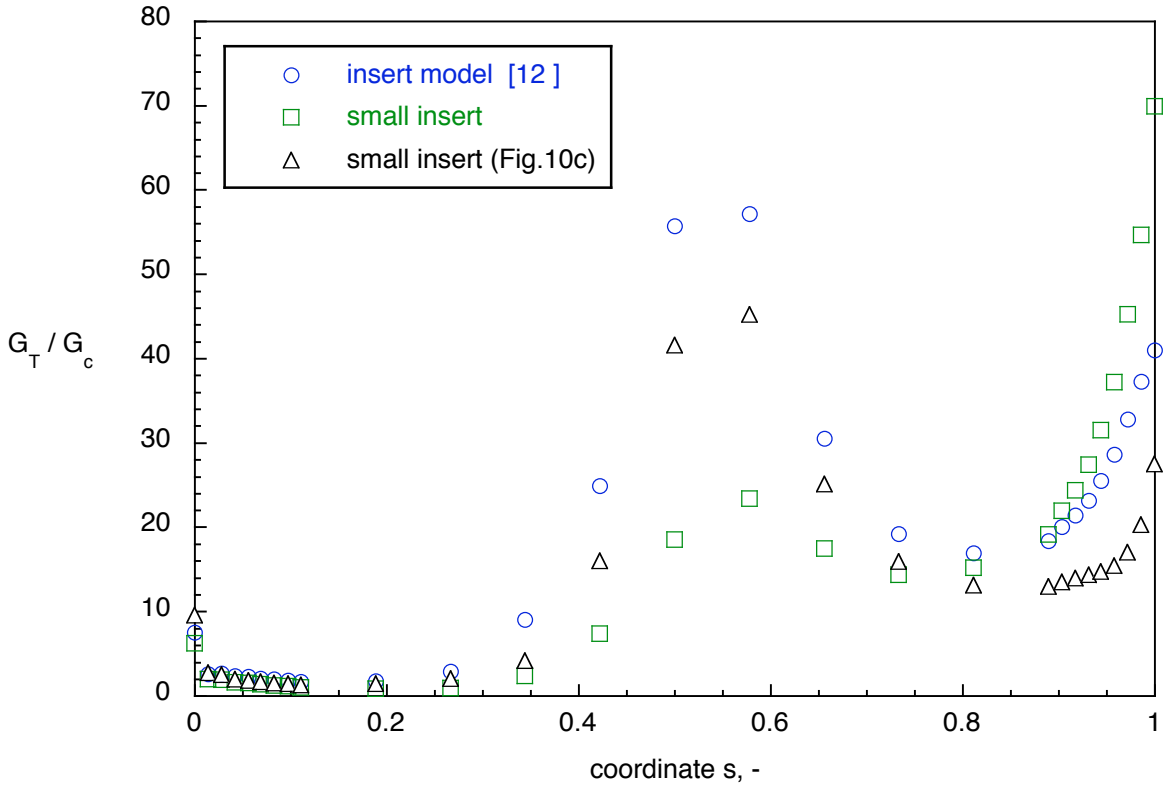

Figure 14. *Computed energy release rate across the width of the stringer for a= 101.6 mm*

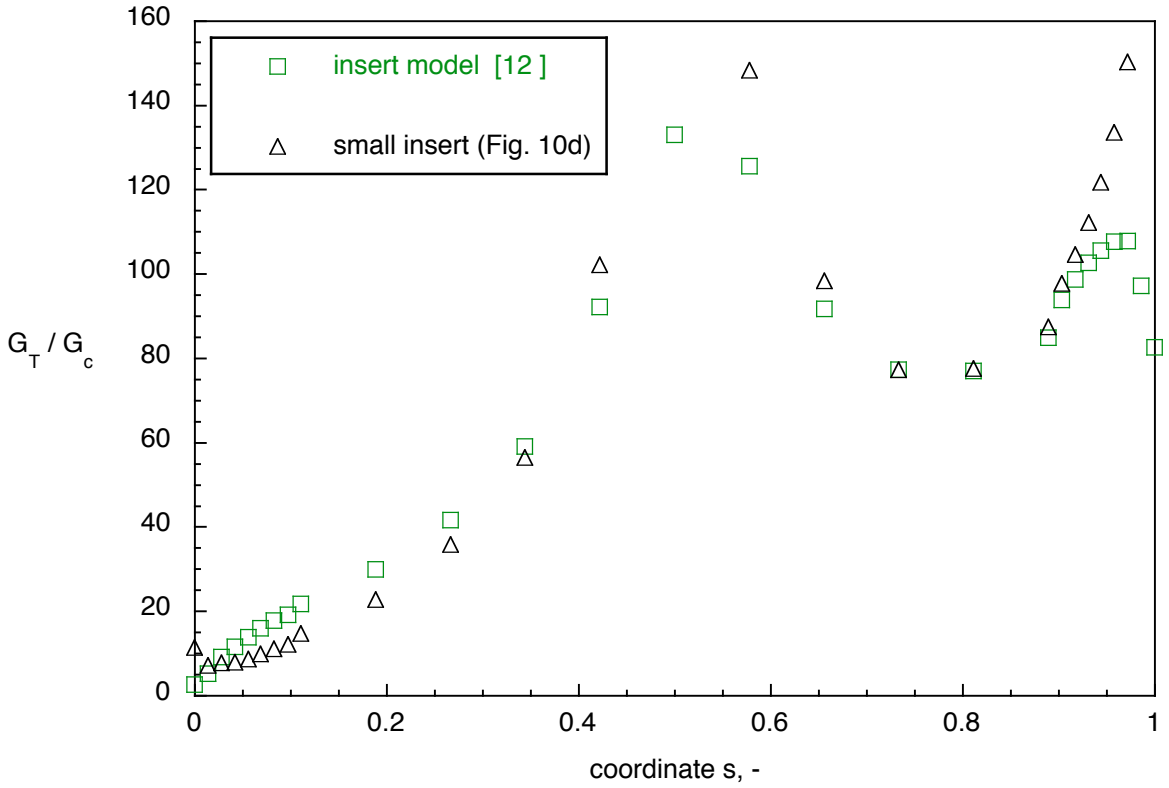

Figure 15. *Computed energy release rate across the width of the stringer for a= 203.2 mm.*

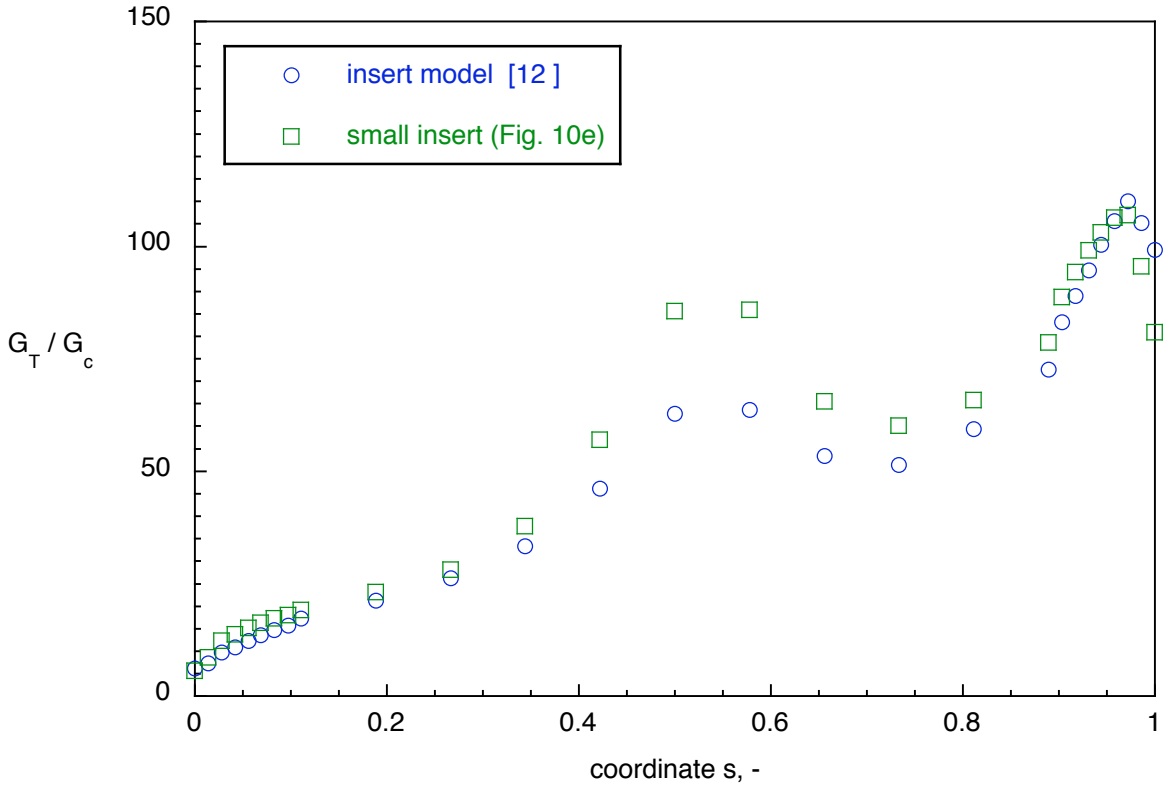

Figure 16. *Computed energy release rate across the width of the stringer for a= 279.4 mm.*

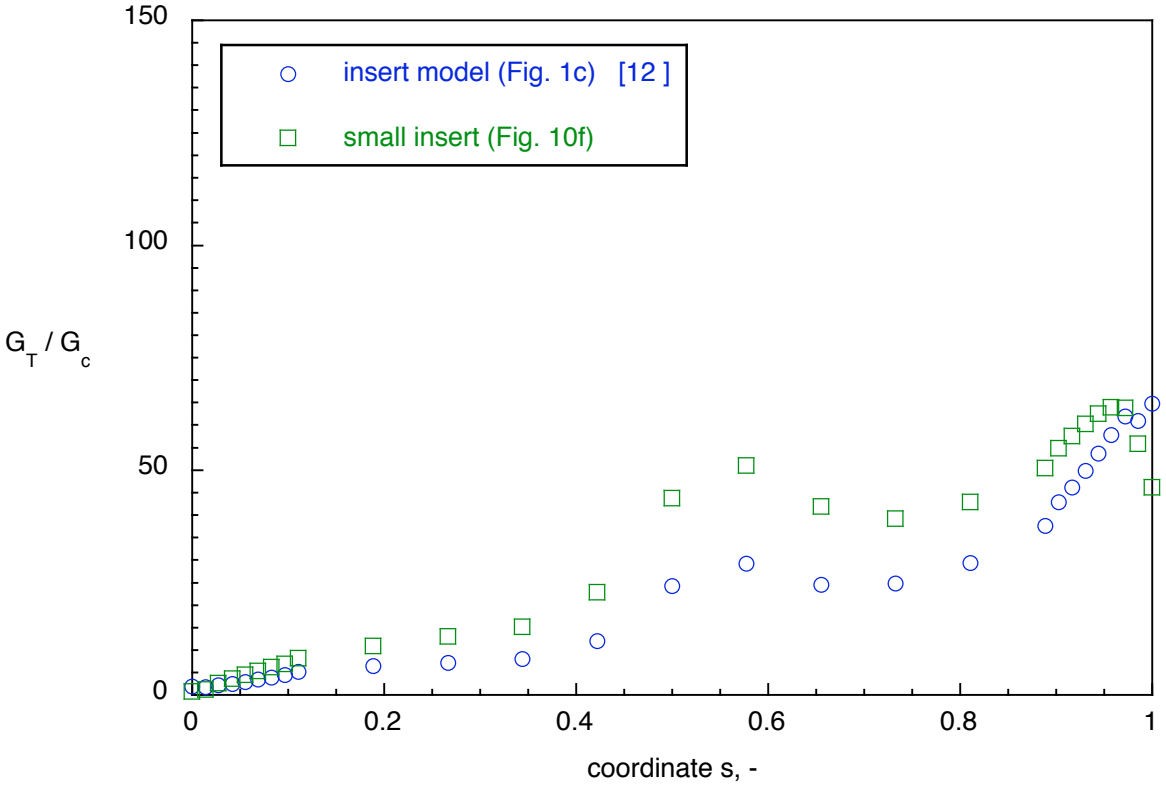

Figure 17. *Computed energy release rate across the width of the stringer for a= 355.6 mm.*

REPORT DOCUMENTATION PAGE

Form Approved
OMB No. 0704-0188

1. REPORT DATE *(DD-MM-YYYY)*	2. REPORT TYPE	3. DATES COVERED *(From - To)*
01/04/2006	Contractor Report	

4. TITLE AND SUBTITLE

Analysis of Composite Panel-Stiffener Debonding Using a Shell/3D Modeling Technique

5a. CONTRACT NUMBER

NAS1-02117

5b. GRANT NUMBER

5c. PROGRAM ELEMENT NUMBER

6. AUTHOR(S)

Ronald Krueger
Pierre J. Minguet

5d. PROJECT NUMBER

5e. TASK NUMBER

1002

5f. WORK UNIT NUMBER

7. PERFORMING ORGANIZATION NAME(S) AND ADDRESS(ES)

NASA Langley Research Center
Hampton, VA 23681-2199

National Institute of Aerospace (NIA)
100 Exploration Way
Hampton, VA 23666

8. PERFORMING ORGANIZATION REPORT NUMBER

NIA Report No. 2006-02

9. SPONSORING/MONITORING AGENCY NAME(S) AND ADDRESS(ES)

National Aeronautics and Space Administration
Washington, DC 20546-0001

10. SPONSORING/MONITOR'S ACRONYM(S)

NASA

11. SPONSORING/MONITORING REPORT NUMBER

NASA/CR-2006-214299

12. DISTRIBUTION/AVAILABILITY STATEMENT

Unclassified - Unlimited
Subject Category 24
Availability: NASA CASI (301) 621-0390

13. SUPPLEMENTARY NOTES

Langley Technical Monitor: Tom Gates

14. ABSTRACT

Interlaminar fracture mechanics has proven useful for characterizing the onset of delaminations in composites and has been used with limited success primarily to investigate onset in fracture toughness specimens and laboratory size coupon type specimens. Future acceptance of the methodology by industry and certification authorities however, requires the successful demonstration of the methodology on structural level. For this purpose a panel was selected that was reinforced with stringers. Shear loading cases the panel to buckle and the resulting out-of-plane deformations initiate skin/stringer separation at the location of an embedded defect. For finite element analysis, the panel and surrounding load fixture were modeled with shell element. A small section of the stringer foot and the panel in the vicinity of the embedded defect were modeled with a local 3D solid model. A failure index was calculated by correlating computed mixed-mode failure criterion of the graphite/epoxy material.

15. SUBJECT TERMS

Composite Material; Skin/Stringer Debonding; Finite Element Analysis; Computational Fracture Mechanics

16. SECURITY CLASSIFICATION OF:			17. LIMITATION OF ABSTRACT	18. NUMBER OF PAGES	19b. NAME OF RESPONSIBLE PERSON
a. REPORT	b. ABSTRACT	c. THIS PAGE			STI Help Desk (email: help@sti.nasa.gov)
U	U	U	UU	30	19b. TELEPHONE NUMBER *(Include area code)*
					(301) 621-0390